

3 MATHUSLA Data Acquisition System and Prototype Module

3.1 MATHUSLA Time of Flight Data Acquisition

The first part of this thesis project focused on testing the capabilities of a CAEN DAQ system for acquiring time of flight (ToF) measurements at nanoscale precision. The emphasis is placed on the use of a commercial off-shelf DAQ due to cost and convenience. As previously discussed in Sec 2.6, each bar in a scintillating layer will have at least one SiPM. If we anticipate about 10 layers for a single module and at least 400 bars for a complete single layer, then there must be enough readout channels to support at least 4000 SiPMs (about 1 SiPM per bar). A customized readout system would take time to design and may be costly, whereas an off-shelf system like the CAEN DAQ is more convenient and easier to scale up to accommodate more SiPMs.

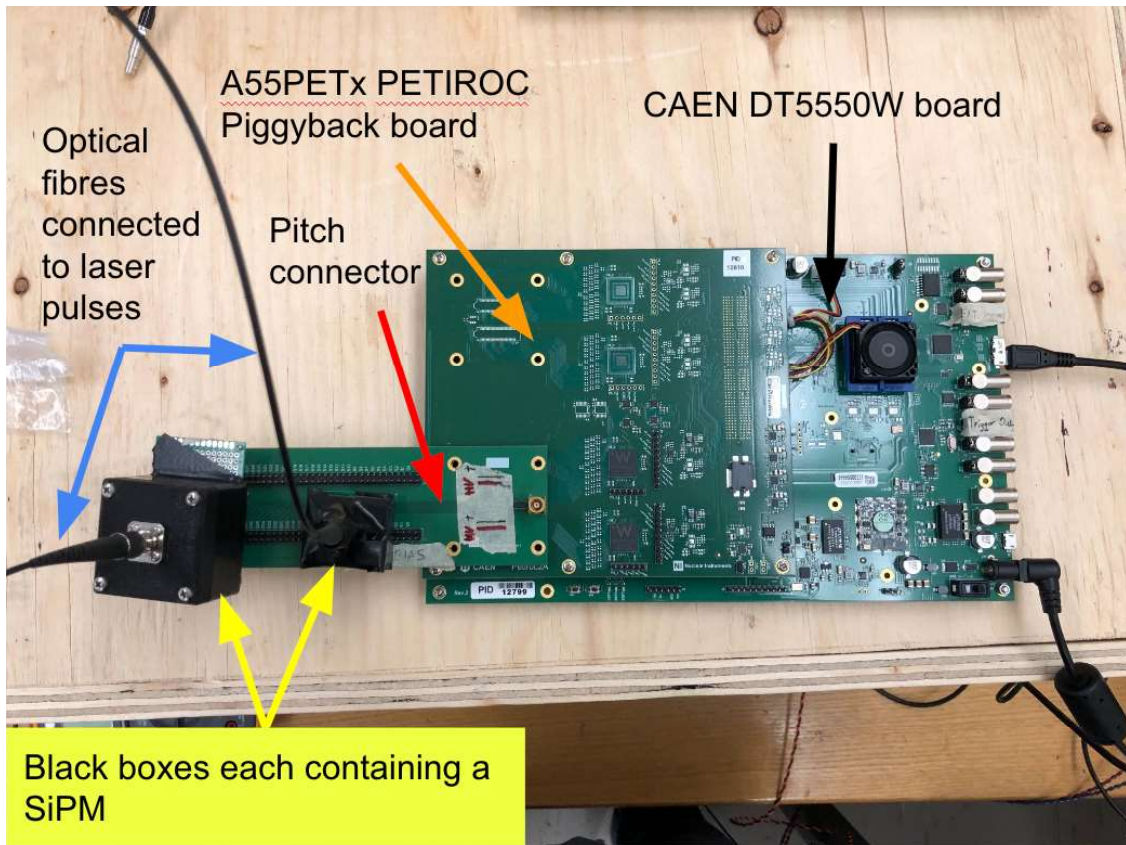


Figure 8: DAQ setup for ToF measurements. Two SiPMs are directly connected to the DAQ, with optical fibres coupled through the black boxes. SiPMs may also be connected with coaxial cable

The apparatus is shown in Figure 8. Two laser pulses were used in conjunction with the CAEN system to measure the ToF of the pulses. The results of the ToF measurements are presented in the following discussion and illustrated inconsistencies with the CAEN DAQ's measurements. A closer examination of the ToF data identified that the CAEN system's analog-to-digital (ADC) converter for fine time measurements is wrong. Additionally, sources of noise that affected the SiPM signal quality in the CAEN system's readout were determined and addressed.

3.1.1 CAEN Data Acquisition System

The DT5550W CAEN board for Weeroc ASICs [5] with the A55PETx PETIROC piggyback board for the DT5550W [5] composes the DAQ system to be tested. An image of the DAQ board setup is shown in Figure 8. The DT5550W motherboard is equipped with a Xilinx Kintex7 FPGA for processing and readout of ASIC signals. The A55PETx PETIROC board supports up to 4 Weeroc ASICs for a maximum of 128 readout channels — 32 channels supported by each ASIC. For simplicity, the combination of the DT5550W motherboard and the A55PETx PETIROC is referred to as the DAQ system. A reverse bias voltage applied across the SiPM is set to 30V with the DAQ software. A time threshold value is also set to discriminate against noise from the DAQ's readout electronics. The time threshold is a minimum voltage value that a detected signal must exceed in order to be considered a valid hit by the DAQ system. The threshold voltage is set according to the equation

$$V_{th} = 0.89V + (10\text{-bit DAC} \cdot 0.92\text{mV}) - (6\text{-bit DAC} \cdot 1.5\text{mV}) \quad (3.1)$$

where the 6-bit digital-to-analog (DAC) value from 0 to 63 is changeable for each channel and the 10-bit DAC value from 0 to 1023 is a global value that is common to all channels. The time delay maps the range of 0 to 255 of an 8-bit DAC to the time range of 27-115 ns; the same delay generated by the 8-bit DAC applies to all readout channels of the DAQ system. The purpose of the time delay is to shift the sampling of the charge signal so that the maximum charge value is measured. For ToF measurements, only the time threshold carries particular significance as it determines what the DAQ system classifies as a hit and initiates the readout process.

The readout process performed by the DAQ board that is relevant to the ToF measurement is illustrated in Figure 9. A SiPM generates an output signal that is delivered to the DAQ board where a pre-amplification of the SiPM's signal is performed — this corresponds to the pre-amp signal in Figure 9. If the pre-amp signal exceeds the time threshold, the time

trigger will be set from off to on and starts the time measurement for an interval of about $20\ \mu\text{s}$. During this counting interval, the coarse counter will count the number of cycles of the 40 MHz clock — up to a maximum of $2^9 = 512$ counts or an interval of $12.8\ \mu\text{s}$. The CAEN manual claims that the coarse counter has a full scale of $20\ \mu\text{s}$, but this appears inconsistent with the fact that the coarse counter is stored in 9 bits. The coarse counter is stored in a 10-bit message where the tenth-bit stores the event's hit information. The fine time conversion begins from the rising edge of the time trigger and ends at the first rising edge of the coarse counter clock after the time trigger signal. The 10-bit fine time ADC maps a range of 5-1019 to an interval of 0-25 ns — underflow and overflow are reserved as 4 and 1020 respectively by the ADC.

Once the readout process begins, no new channel on the same ASIC can trigger another readout process. Instead, any subsequent hits will be grouped in the same event as part of the initial hit. Following the $12.8\ \mu\text{s}$ counting interval, a $\sim 12\ \mu\text{s}$ dead time is triggered to allow for the data to be read out from the DAQ. The conversion and data serialization process will take a total of $\sim 25\ \mu\text{s}$ which means that the maximum trigger rate for each event is about 40 kHz [5]. The data serialization is shown in Figure 10. No new hits will be triggered on the ASIC sending data out during the dead time.

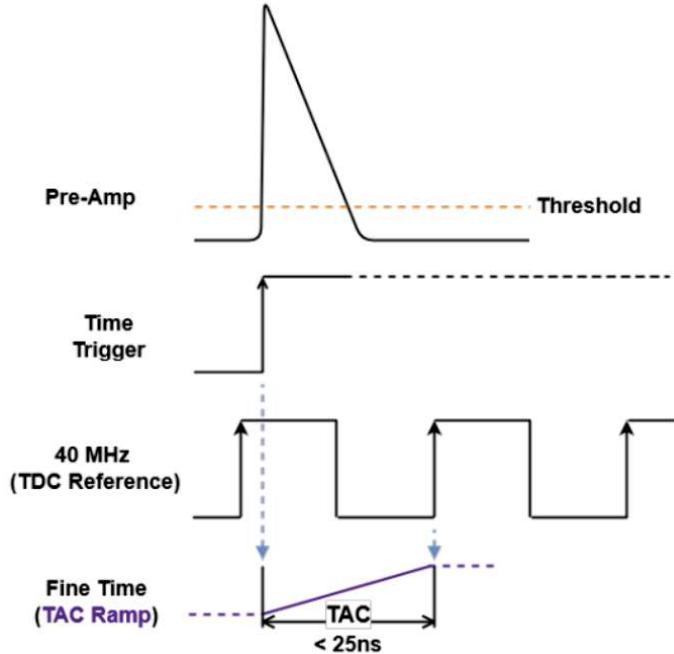


Figure 9: ASIC readout process for time measurements using the DAQ's default photon hardware scheme [5, Fig. 11.1]

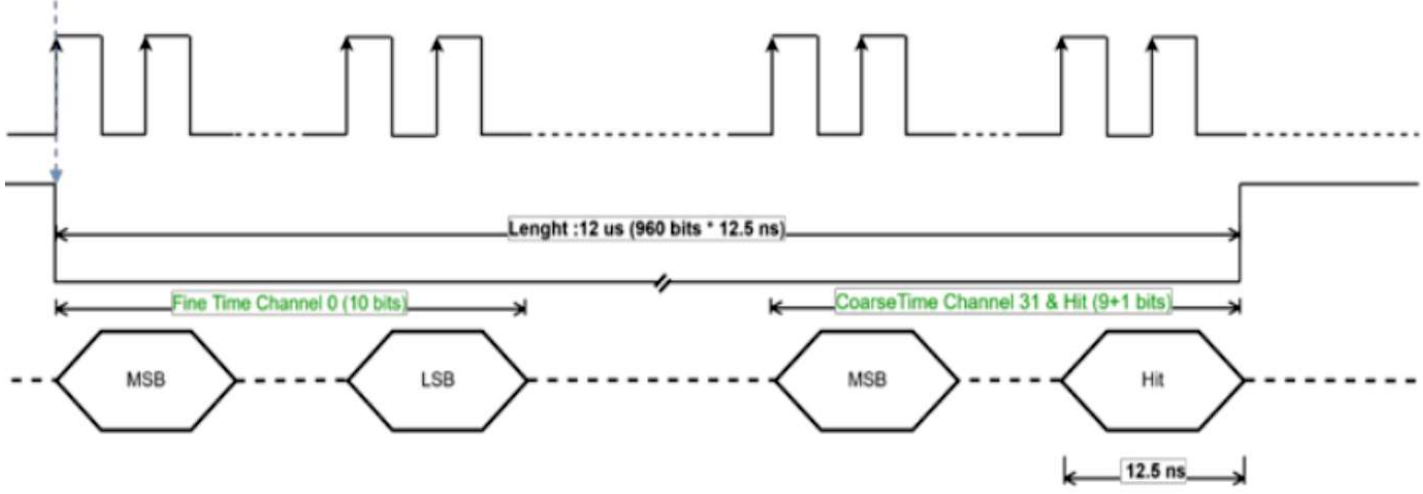


Figure 10: ADC data serialization for output transfer. The top line is a 160 MHz periodic clock that is sampled by the FPGA on the DT5550W board. The following line indicates if the signal is being transmitted — switches from 1 to 0 when the data is being serialized. The last line is the out signal line that shows how the serialized data is outputted. Each bit requires 12.5 ns to deliver. [5, Fig. 11.1]

The ToF is calculated from the data output of the DAQ with the following equation:

$$ToF = ((coarse_1 + 1) \times 25 \text{ ns} - fine_1) - ((coarse_2 + 1) \times 25 \text{ ns} - fine_2) \quad (3.2)$$

where *coarse* values are the coarse time counter values for each channel and the *fine* values are the fine time counter values for each channel. Multiplying by 25 ns is to convert the digital coarse counter values into time values. Moreover, because the fine time counter was effectively converted from an analog to a digital value, the conversion for the DAQ's output into time values is as follows:

$$fine_{ns} = (fine - fine_{min}) \times \alpha \quad (3.3)$$

$$\alpha = \frac{25 \text{ ns}}{fine_{max} - fine_{min}} \quad (3.4)$$

where *fine_{max}* and *fine_{min}* are the maximum and minimum values from the DAQ output data set for a channel that captured real hit events and *fine* represents the fine counter values for the same channel from the DAQ data output.

Some necessary offline pre-filtering of the output needs to be performed prior to computing the ToF. Firstly, channels that self-trigger on noise inherent to their channels will typically register hits with a value of 0 or not a number (NaN). Only a value of 1 in the

channel hit column is considered a valid detection. Any channel which has a total number of valid hits greater than or equal to 1% of all the events collected in a data run is considered for ToF measurements. From the channels of interest, events, where the channel has a hit with a value of 0 or NaN, should be removed. This way, we ensure that our ToF is calculated from events where the channels of interest were properly triggered by some external interaction rather than electronic noise.

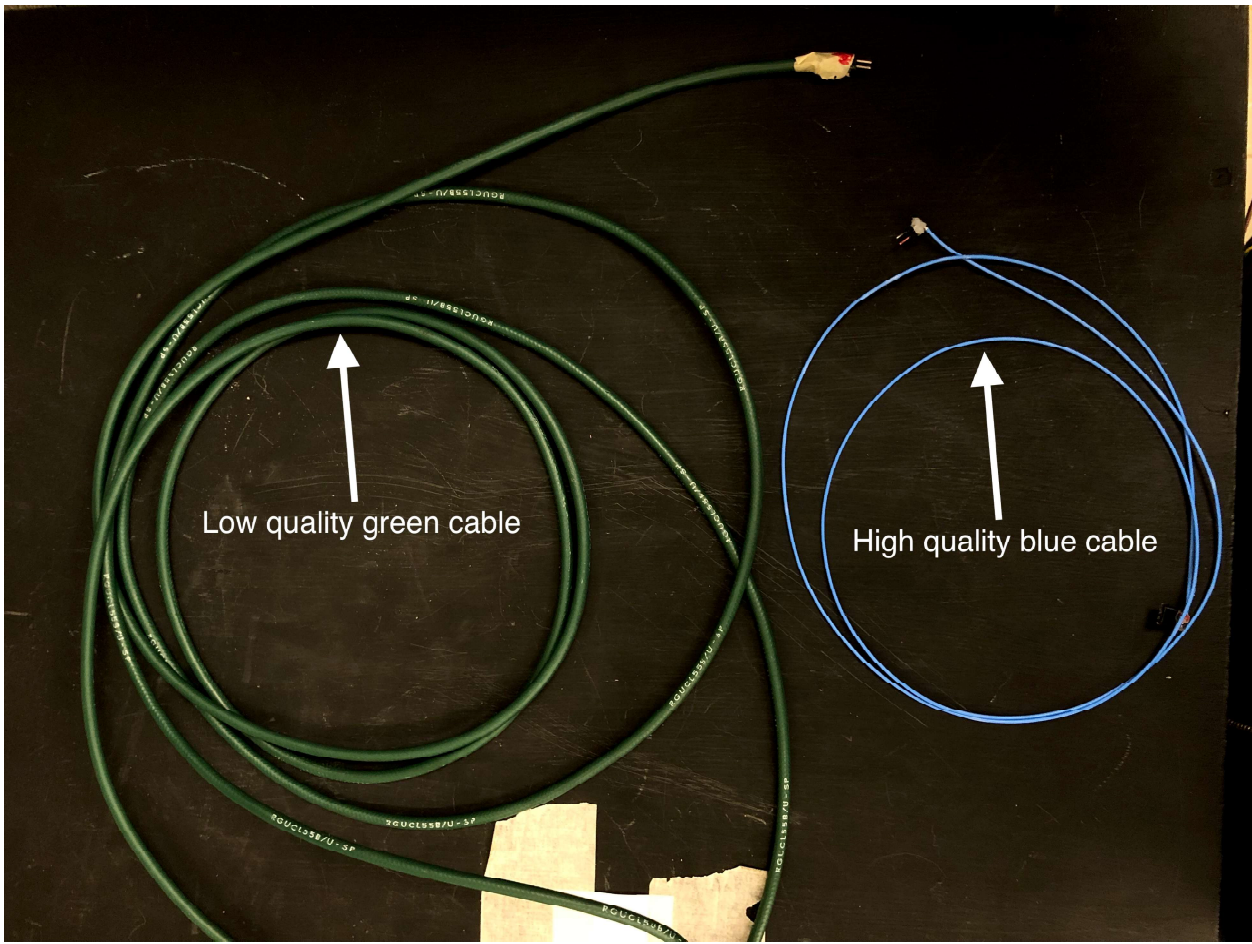
Lastly, it should be noted that a challenge with the CAEN DAQ system does seem to be related to quality control. About 12 channels (6 channels per ASIC) were determined to be broken as they were triggered randomly on noise sources. There appeared to be about 1 broken channel every month for unknown reasons. The broken DAQ was sent in for repairs and a new DAQ with 4 ASIC chips was purchased as well. It was immediately found that the new DAQ had 4 channels that were connected together for one of the ASIC chips. While collecting a large data set with more than 100,000 events, two of the ASIC chips on the new DAQ broke — all channels for the broken ASICs were triggering on noise sources. Some potential causes for the channels to break could be the improper grounding of the DAQ, accidental shorting of channels, and quality control of the product. Further discussions with CAEN are needed to pinpoint the usage issues and reduce the frequency of channels breaking. In the next section, we examine some possible sources of noise that arose from the apparatus.

3.1.2 Noise Reduction of SiPM Pre-amplifier Signal

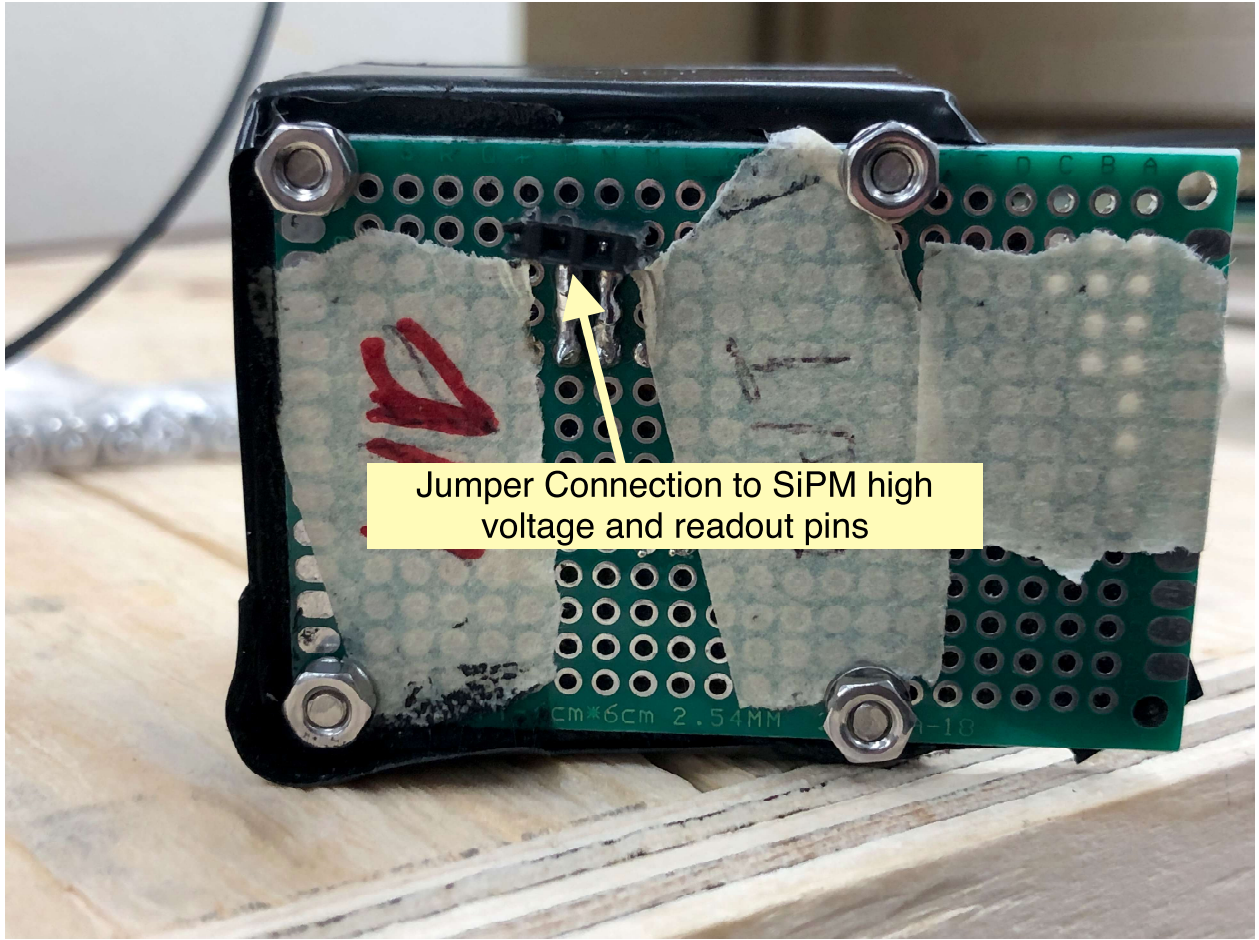
In order to achieve good timing resolution, it was necessary to ensure that the pre-amplifier signal from the SiPM was de-noised and free of low-frequency noise sources. The causes of noise can be attributed to several factors. Some possible sources of noise include interference between ASIC channels, noise introduced from poor coaxial cable connections and poor coupling between the WLS fibre and SiPM. Here, we will not consider interference between ASIC channels since this is a manufacturing-related issue that has no simple solution with available lab equipment. Poor coupling between the WLS fibre and SiPM is not a huge concern in the apparatus of Figure 8 as the optical fibre that connects the laser pulse to the black box is screwed on. Hence, we investigate the coaxial cable connection from SiPM to DAQ.

The different connection methods that were used are shown in Figure 11. In the ideal case, the best signal would be obtained by directly connecting the SiPM to the DAQ. However, in the actual MATHUSLA detector, it will be impossible to avoid wired connections from the SiPM to the DAQ due to the size of the module and the number of readout channels.

Wires can introduce noise in the signal through self-induction or because of poor impedance matching of the signal frequency with the material's characteristic impedance — these effects become more significant as the wire length increases and becomes comparable to the signal's wavelength. Since the pre-amplifier signal is a low-frequency signal on the order of 10-100 MHz, wire lengths between about 3-30 m can introduce impedance-matching challenges. The impedance of the coaxial cable connectors depends on their cladding material. In the DAQ testing apparatus, wire lengths did not quite reach the 3-30 m range. Therefore, it was more important to investigate the cladding quality as the main source of noise rather than cable length.



(a) High-quality blue coaxial cable and low-quality green cable connectors for the SiPM to the DAQ



(b) Jumper direct connection from the SiPM to the DAQ

Figure 11: Different connection methods for SiPM to the DAQ

The amplitude of the pre-amplifier signal is critical for all DAQ measurements. No timing measurement process can begin until the pre-amplifier signal exceeds the time threshold and initiates the measurement process. The pre-amplifier signal that is output from the DAQ is shown in Figure 13. The signal is inverted on output, which is why it appears negative — the DAQ’s internal processing sees the signal as positive. When low-frequency noise is introduced, the signal’s maximum voltage amplitude decreases. Too much external noise may cause the DAQ to not detect actual hits on the SiPM. In Figure 13c, the pre-amplifier signal has more oscillations coupled into it than the direct connect and high-quality coaxial cable connections. Additionally, the oscillations in Figure 13c have shifted where the voltage peak appears in the signal as well as the value of the peak — a measurement of its amplitude is also affected. In comparison, the trace of the high-quality coaxial cable is quite similar to that of the ideal signal of a directly connected SiPM. These observations suggest that there is indeed a significant difference in signal quality with different cables.

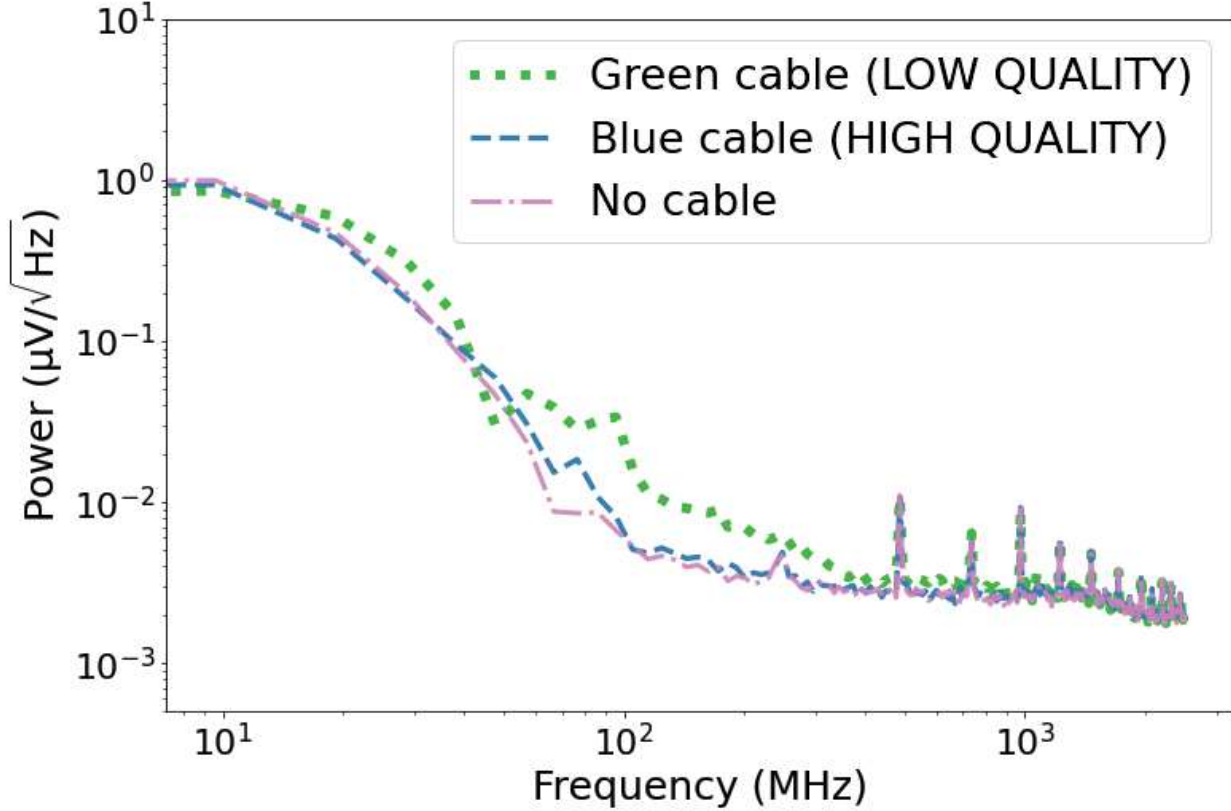
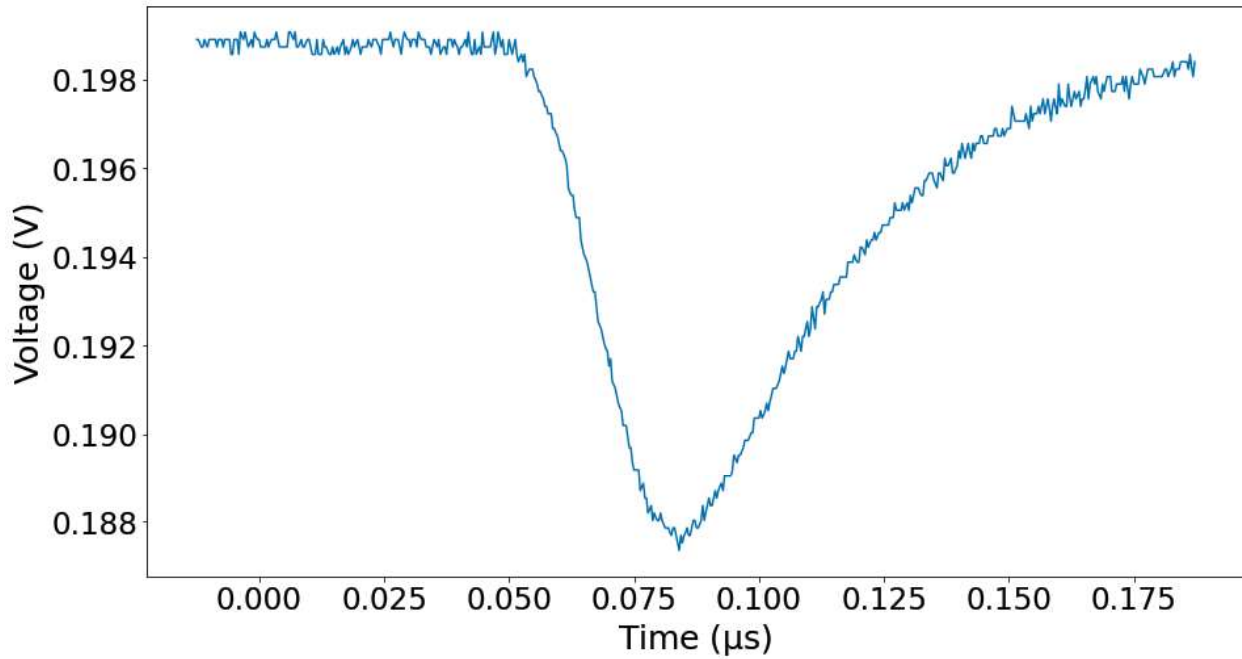
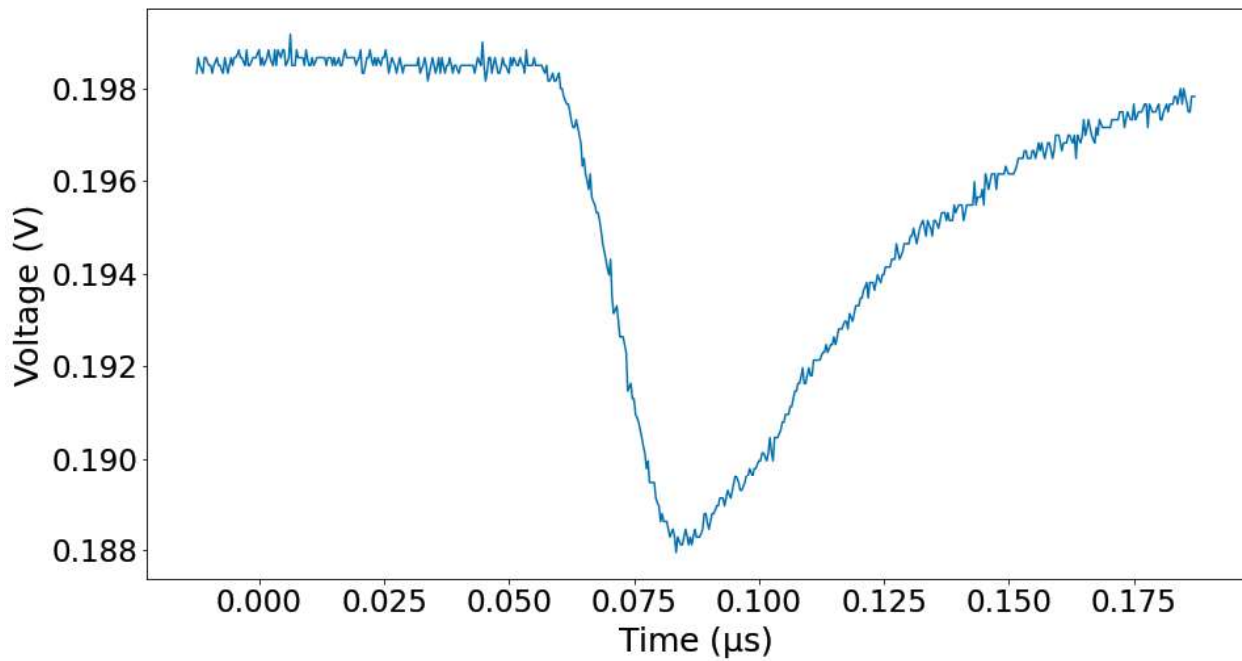


Figure 12: Average noise in the frequency spectrum for the pre-amplifier signal of the 3 different connection types. 100 pre-amplifier signals were averaged for each connection type

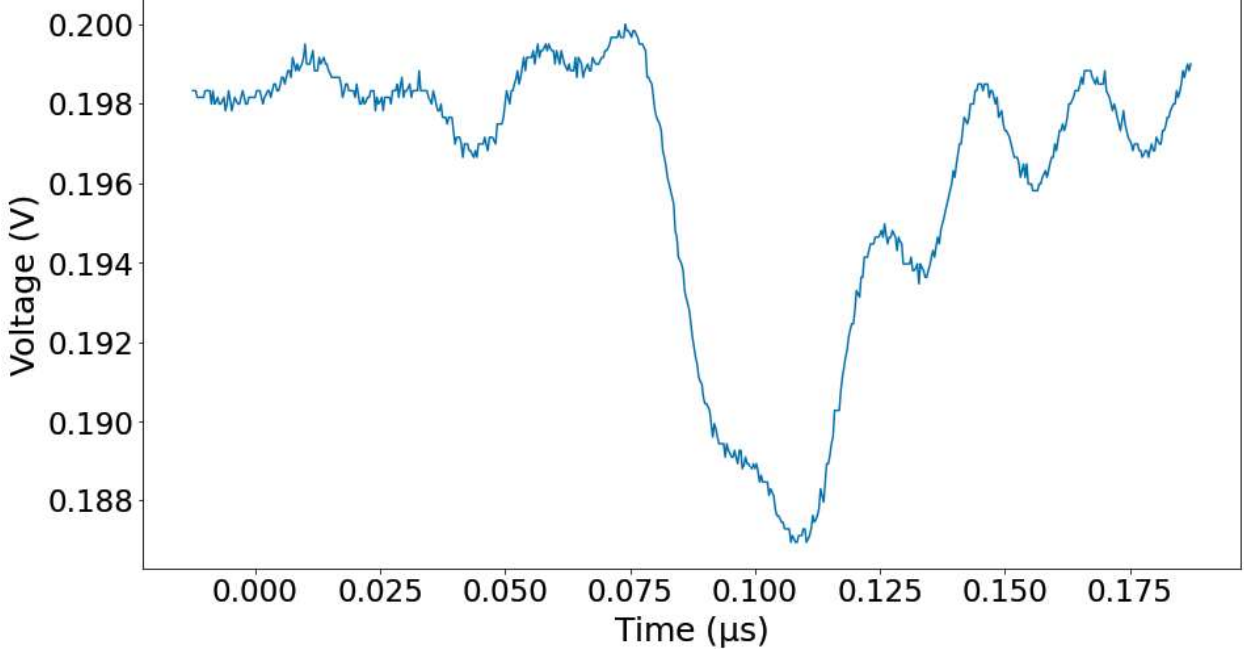
The noise plot in Figure 12 of the pre-amplifier signals further shows that the low-quality cable introduces more low-frequency noise than the other connections. At high frequencies, the noise is essentially identical for the three connections and has a sufficiently low amplitude that it will not interfere with the overall pre-amplifier signal. In Figure 13, the high-frequency (larger than 400 MHz) noise can actually be observed as small and rapid squiggles throughout the signal. When examining the region between 10-100 MHz, the low-quality cable is about 3 times larger than the high-quality cable and direct connection in the range from 50-200 MHz. This does coincide with the fact that the pre-amplifier signal in Figure 13c has more oscillations.



(a) Pre-amplifier signal from a SiPM directly connected to the DAQ



(b) Pre-amplifier signal from a SiPM connected to the DAQ with a high-quality coaxial cable



(c) Pre-amplifier signal from a SiPM connected to the DAQ with a low-quality coaxial cable

Figure 13: Different pre-amplifier signal outputs from the DAQ due to different SiPM connections

Based on the above observations, it was decided that only the direct connection or high-quality cabling would be used to connect the SiPM to the DAQ for ToF measurement tests. Moreover, when designing the cabling of the overall MATHUSLA detector module, it will be important to also consider the impact that cable shielding may have on the SiPM signal being delivered to the DAQ. Additionally, with the scale of the MATHUSLA detector module, the length of the cabling may also be on a similar length scale as the wavelength of the SiPM signal and adds an additional level of consideration for noise sources.

3.1.3 Time of Flight Results

Before discussing the ToF measurement results from the DAQ testing, we present a brief discussion on how ToF can be used in particle track reconstruction. Figure 14 shows a simplified schematic diagram for using ToF to determine where an incoming particle collided with the scintillating layer.

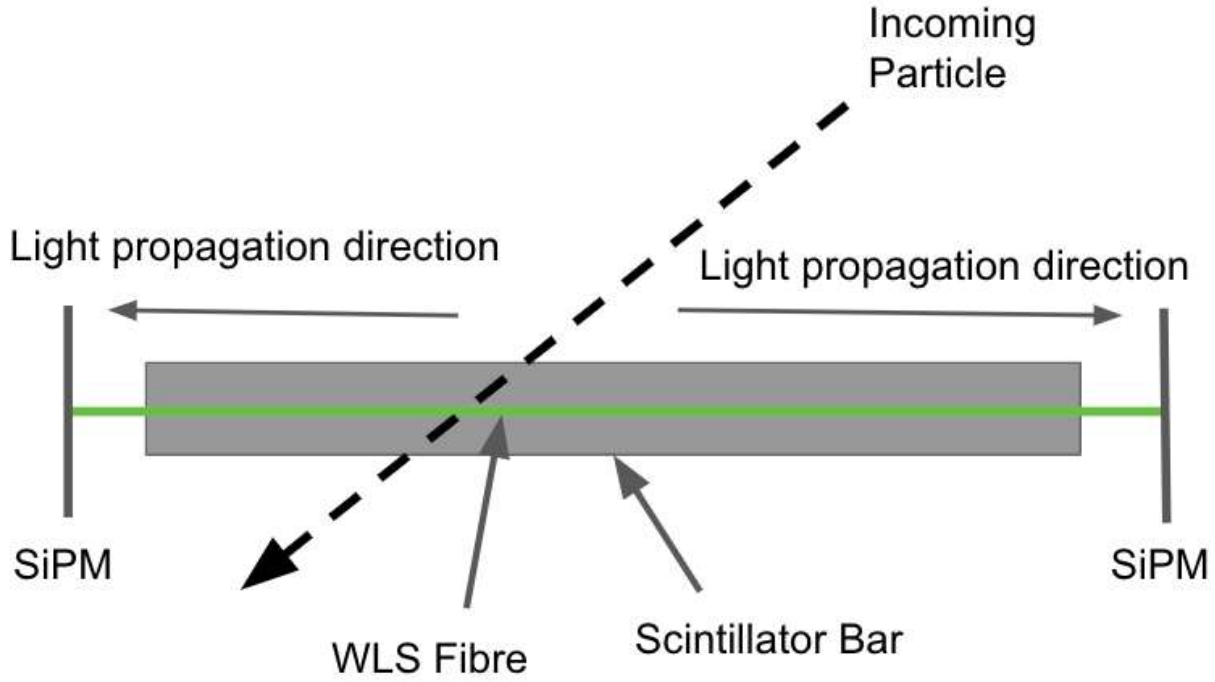


Figure 14: Simplified diagram of how the time of flight measurements can be used to determine the position where a particle interacts with the scintillating layer

Let the bar length be L , the distance from the right end of the bar to where the incoming particle's trajectory intersects with the bar be d , the time to propagate from the particle's intersection point to the left of the bar be t_1 and the time to propagate from the particle's intersection point to the right of the bar be t_2 . Also, assume that light in the WLS fibre travels at the vacuum speed of light c . From the schematic in Figure 14, we can see that the left SiPM will detect and be triggered by a signal from the WLS fibre before the right SiPM. Therefore, d can be computed as follows:

$$\begin{cases} d = ct_2 \\ L - d = ct_1 \end{cases} \quad (3.5)$$

$$\implies 2d - L = c(t_2 - t_1) \quad (3.6)$$

$$2d - L = c\Delta t \quad (3.7)$$

$$d = \frac{c\Delta t + L}{2} \quad (3.8)$$

Hence, the position where the particle's trajectory intersects with the scintillator can be computed if we know the length of the bar, speed of light propagating in the WLS fibre, and the ToF ($\Delta t = t_2 - t_1$). This simple result demonstrates how the ToF can be used in the track reconstruction of an incoming particle as it passes through multiple detection

planes. Additionally, because the length of the bars and the WLS fibres will be typically on the order of $\mathcal{O}(10 \text{ m})$ — we refer to the length of WLS fibres threaded through 1-2 bars and not the total WLS fibre length to be used in the detector — the expected timescale will be nanoseconds. Therefore, it is very important that the ToF measurements be precise to at least 1 ns for good track reconstruction.

The testing apparatus setup is shown in Figure 8. One LED was connected to the oscilloscope and another was connected to a PCO-7114 laser pulsar board. The frequency of the laser pulse was determined by the wave generator on the oscilloscope — the same pulsing frequency was delivered to the laser pulsar board. The LED laser light was delivered to the SiPM black boxes via optical cables. LEMO cables can be added to delay the delivery of a laser pulse to one of the SiPMs. The expected distribution of the ToF measurements would be a very narrow Gaussian curve about the time difference between the two channels. Figure 15 shows a measurement of the ToF conducted with the DAQ. From visual inspection, the distribution does resemble a normal distribution but the bump at around 30 ns is unexpected. The distribution was fit to the equation of a Gaussian distribution

$$f(x) = P_0 e^{-\frac{1}{2}(\frac{x - P_1}{P_2})^2} \quad (3.9)$$

where P_0, P_1, P_2 are fitting parameters; P_1 and P_2 represent the mean and standard deviation respectively and are the parameters of interest. The orange curve in Figure 15 is the best fit with parameters and fit statistics:

$$P_1 = 33.06 \quad (3.10)$$

$$P_2 = 1.12 \quad (3.11)$$

$$\chi^2/\text{dof} = 1.58424 \quad (3.12)$$

So, the ToF is about (33.06 ± 1.12) ns and the $\chi^2/\text{dof} = 1.58424$ is somewhat close to 1 which suggests the fit is reasonably appropriate and that the uncertainties have not been overestimated. The uncertainty chosen on the counts per bin was $\sigma_{\text{counts in each bin}} = 15$ — this was chosen to account for fluctuations from the DAQ triggering on noise events.

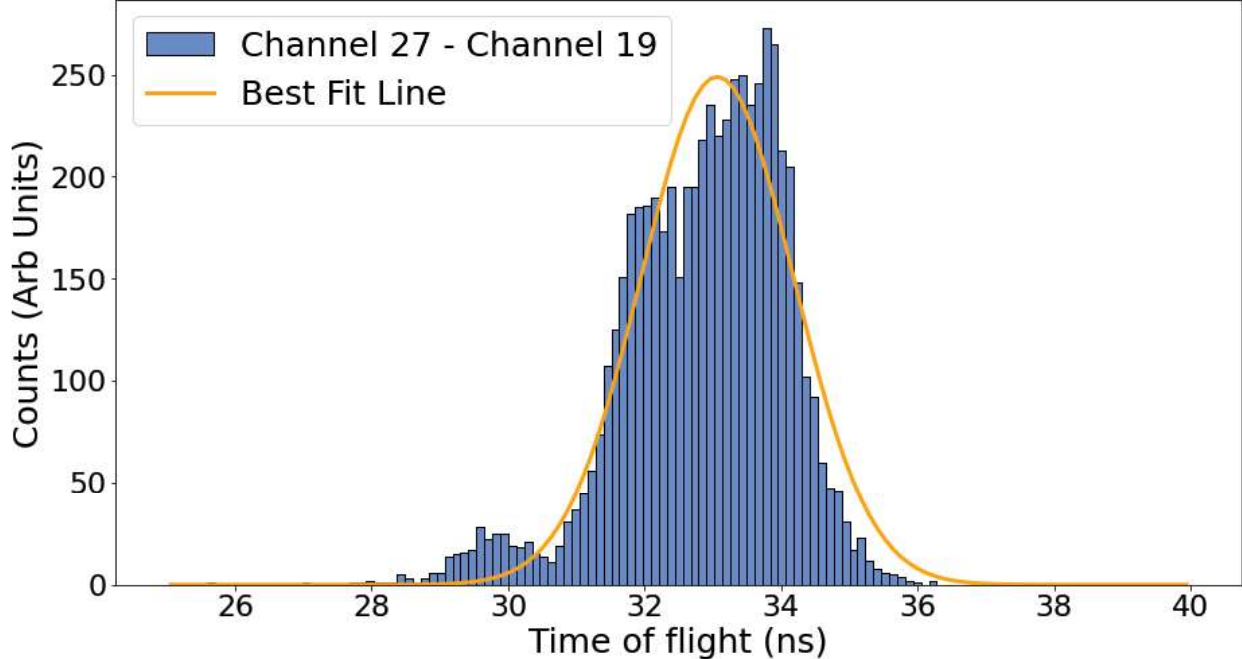


Figure 15: ToF measurement between Channel 27 and Channel 19 on the same ASIC chip. Channel 19 is the triggering channel in this measurement. A Gaussian best-fit function is shown as well

Although the distribution obtained in Figure 15 is reasonably Gaussian, it is still irregular and not as consistent as expected. In fact, many of the ToF results would have more than one significant peak. Figure 16 shows a bimodal distribution. The Gaussian best fit has parameters and fit statistics:

$$P_1 = 27.56 \quad (3.13)$$

$$P_2 = 1.72 \quad (3.14)$$

$$\chi^2/\text{dof} = 27.50560 \quad (3.15)$$

The ToF is about (27.56 ± 1.72) ns and the $\chi^2/\text{dof} = 27.50560$ is much larger than 1. The fit statistics suggest that the Gaussian function is not a great description of the distribution — which also agrees with a visual inspection of the distribution. This non-Gaussian plot deviates from the type of distribution we would expect.

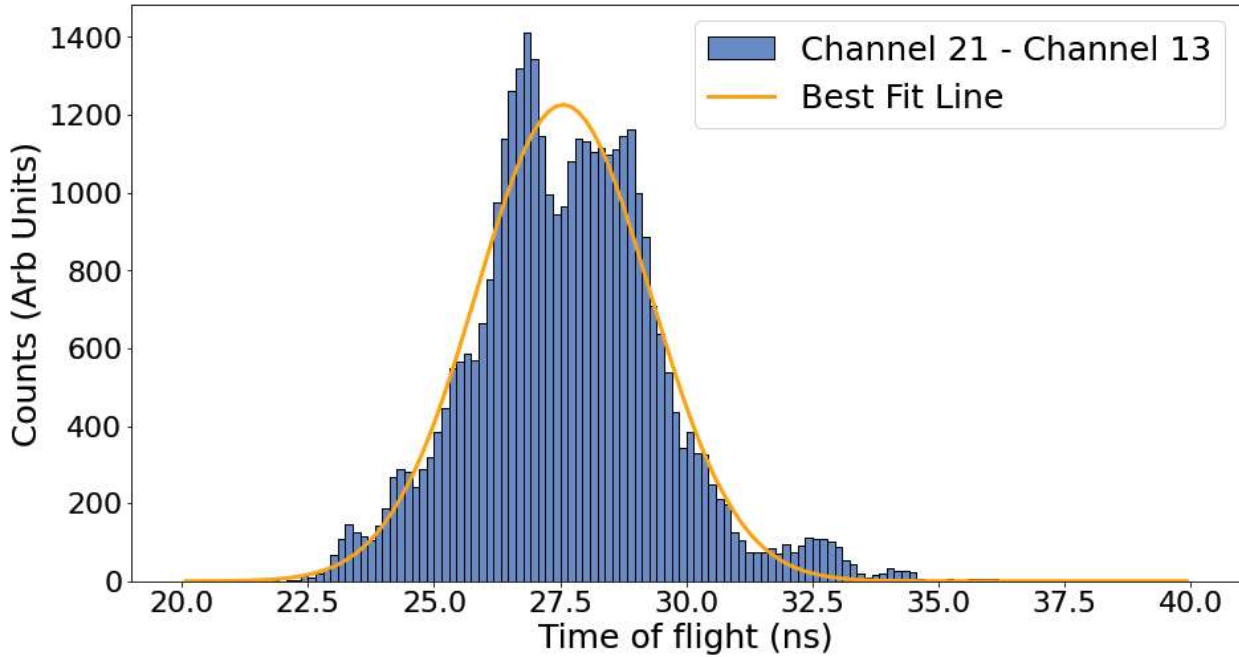
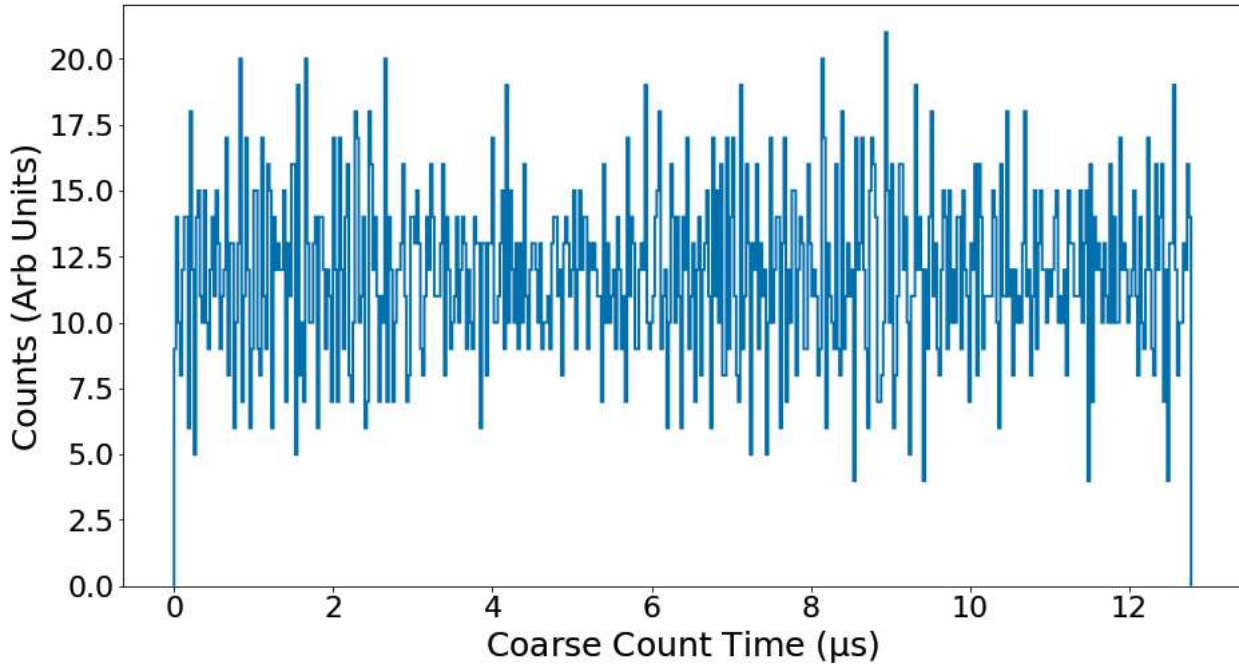
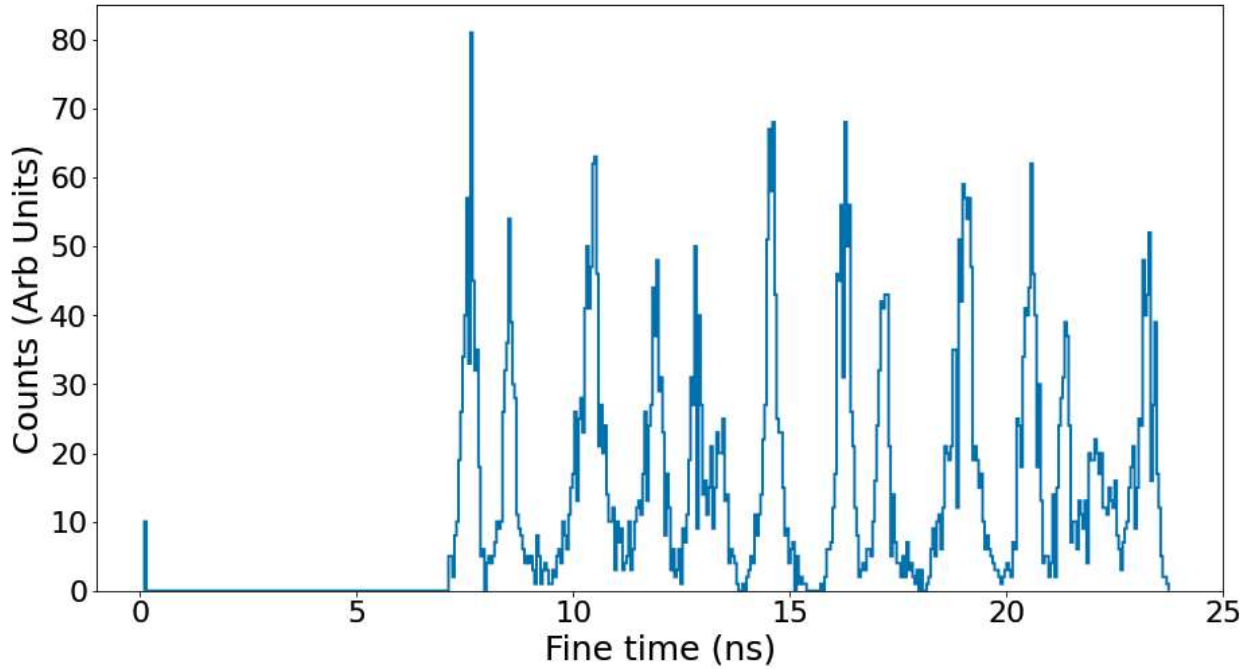


Figure 16: ToF measurement between Channel 21 and Channel 13 on the same ASIC chip. Channel 13 is the triggering channel in this measurement. A Gaussian best-fit function is shown as well

Measurements of the ToF are dependent on the coarse counter and fine time converter in the DAQ. In the setup, the laser pulses' triggering signal and the DAQ clock were not synchronized. As a result, it would be expected that the DAQ itself would be triggered at random times and produce uniform distributions for the coarse counter times and the fine times. When computing the ToF from Equation 3.2, the majority of values should coincide with the ToF while some spread is expected as a result of laser signals not firing exactly at the same moment as the triggering signal's rising edge. In Figure 17, the coarse counter distribution does match what we would expect of a uniform distribution — integrating the normalized distribution yields 0.9982, which is very close to 1 as expected. On the other hand, the fine time converter shown in Figure 17b is completely unexpected. Not only is the distribution inconsistent with a uniform distribution, but it also appears to be exhibiting peaks at specific values. Moreover, the fine time is measured in nanoseconds and on the same scale as the ToF values. Therefore, the unexpected fine distribution is the most likely cause for the non-Gaussian distributions of the ToF measurements.



(a) Coarse counter histogram for Channel 19 in Figure 15



(b) Fine conversion histogram for Channel 19 in Figure 15

Figure 17: Coarse counter and fine time conversion histograms for Channel 19 in Figure 15

We investigated the fine time further by recording the fine time converter's ADC voltage values from the oscilloscope — the purpose was to determine whether the ADC

conversion introduces the irregular distribution or whether a different hardware conversion issue in the DAQ was at fault. Figure 18 also shows the non-uniform and spiked distribution observed in Figure 17b. Hence, it suggests that this particular fine time issue is related to the fine time's ADC ramp conversion. Presently, there is no solution that satisfactorily resolves this problem. In consultation with the CAEN support team, it was suggested that a similar problem had been observed by their team and that it was caused by the pre-amplifier signal's rising edge taking too long to reach its maximum. The CAEN team suggested testing with a faster SiPM that could rise to its maximum in under 5 ns.

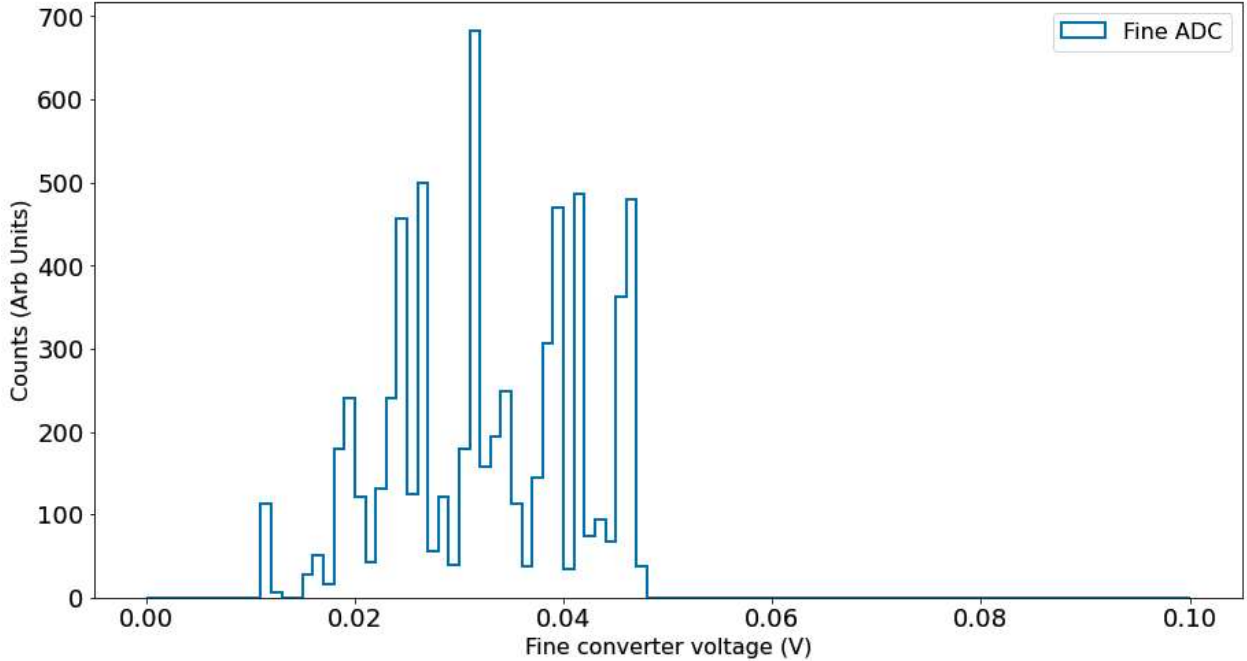


Figure 18: Fine time ADC ramp voltage histogram. ADC ramp voltage was obtained from the ADC ramp output option of the DAQ

3.2 MATHUSLA Prototype Module

The second half of the project was directed toward the design and construction of a small-scale prototype of the detector module to be used in MATHUSLA. A design for the frame of the detector module was proposed to ensure stability and sturdiness, allow for easy installation of scintillator layers and also have an adjustable height parameter. Progress and current completion of the prototype module is presented in the discussion. To support the installation of the scintillator layers, a design for a connection piece to the module frame is proposed. Lastly, a simple mechanical solution is presented to hold the WLS fibres flush against the SiPMs to avoid poor coupling.

3.2.1 Module Frame Design

In designing the module frame, there are 6 main items that the module prototype should possess:

1. **Prototype module similarity to proposed MATHUSLA module design.** The purpose of the prototype is to serve as a small-scale imitation of the module that will be installed in MATHUSLA. In order for tests on the prototype to be comparable to MATHUSLA modules, the MATHUSLA module needs to be replicated as closely as possible. Additionally, it also is an opportunity to evaluate possible shortcomings in the module design and where improvements can be made.
2. **Prototype module is easy to level and stabilize.** One of the useful attributes of the MATHUSLA detector's vertical design is that it provides good rejection against background signals. As such, it is important that scintillating layers in the module be parallel to one another — ideally, it would be level with the floor. Therefore, the prototype module should be easy enough to manipulate so such layers can be made level. Additionally, the module should also be stable. Wobbling during operation could affect the reconstruction of particle tracks that collide with the layer and lead to erroneous conclusions.
3. **Prototype module has an adjustable height.** One of the factors that can be tested with the prototype is how different scintillator layer spacing can affect the detection and reconstruction of particle tracks. An adjustable height will make it possible to easily test different possible layer spacing by altering the module height. Additionally, being able to adjust the module height also facilitates easier assembly.
4. **Prototype module is durable and can support its own weight when fully extended.** The prototype cannot collapse under its own weight. When the module is raised to its full height, it needs to be able to support the weight of the upper tracking layer frame — this is a minimum requirement as the addition of the scintillator layers will add more weight. It would be desirable for the prototype to be able to support at least 1.5 times the weight of its frame; this builds in a tolerance of about 0.5 times the weight of the frame for scintillating layers.
5. **Prototype module makes adjusting scintillator layers easy.** Related to elements 2 and 3, the prototype should have an easy mechanism to connect scintillator layers

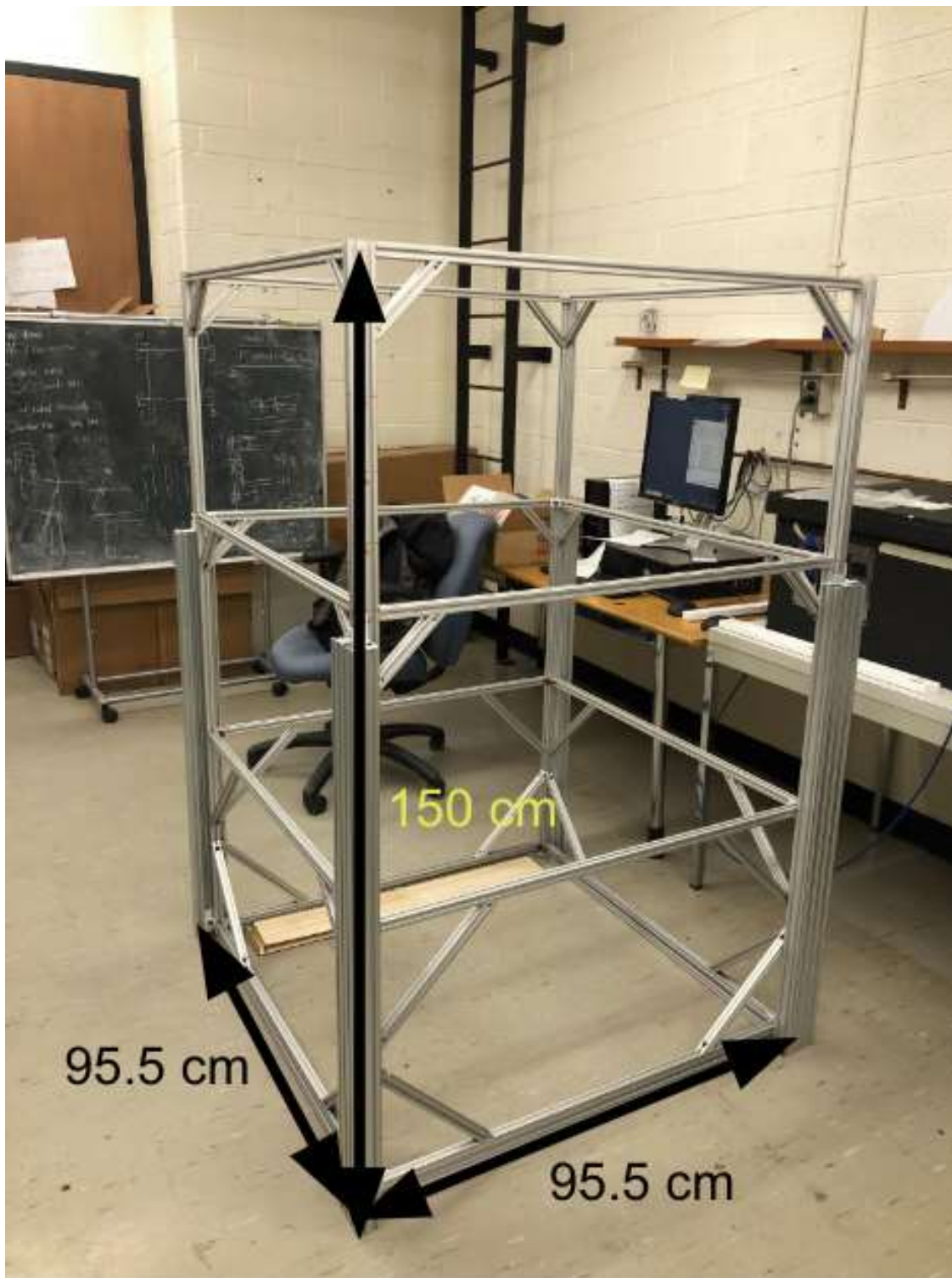
to the frame and modify the attached layers without the need for removal. If the scintillator layers are easy to adjust, levelling the layers will be much easier. Similarly, changing the layer spacing will be less of a hassle if the layer connection to the prototype is simple. However, making scintillator layers easy to adjust at the expense of a reliable connection of the layer to the prototype frame is undesired — the connection between layer and module must be able to support the weight of about 20 plastic scintillating bars.

6. **Prototype module will allow for easy and organized electronics readout connections.** Since each scintillator will possess many SiPMs that need to be connected to readout channels on a DAQ, it is imperative that good cable management is maintained to avoid interference between different readout signals. The prototype should be designed so that cable management is easy — at least, the design can be modified to manage cables. Moreover, the DAQ should be situated on the prototype so that connections from all scintillator layer SiPMs require the least amount of cabling.

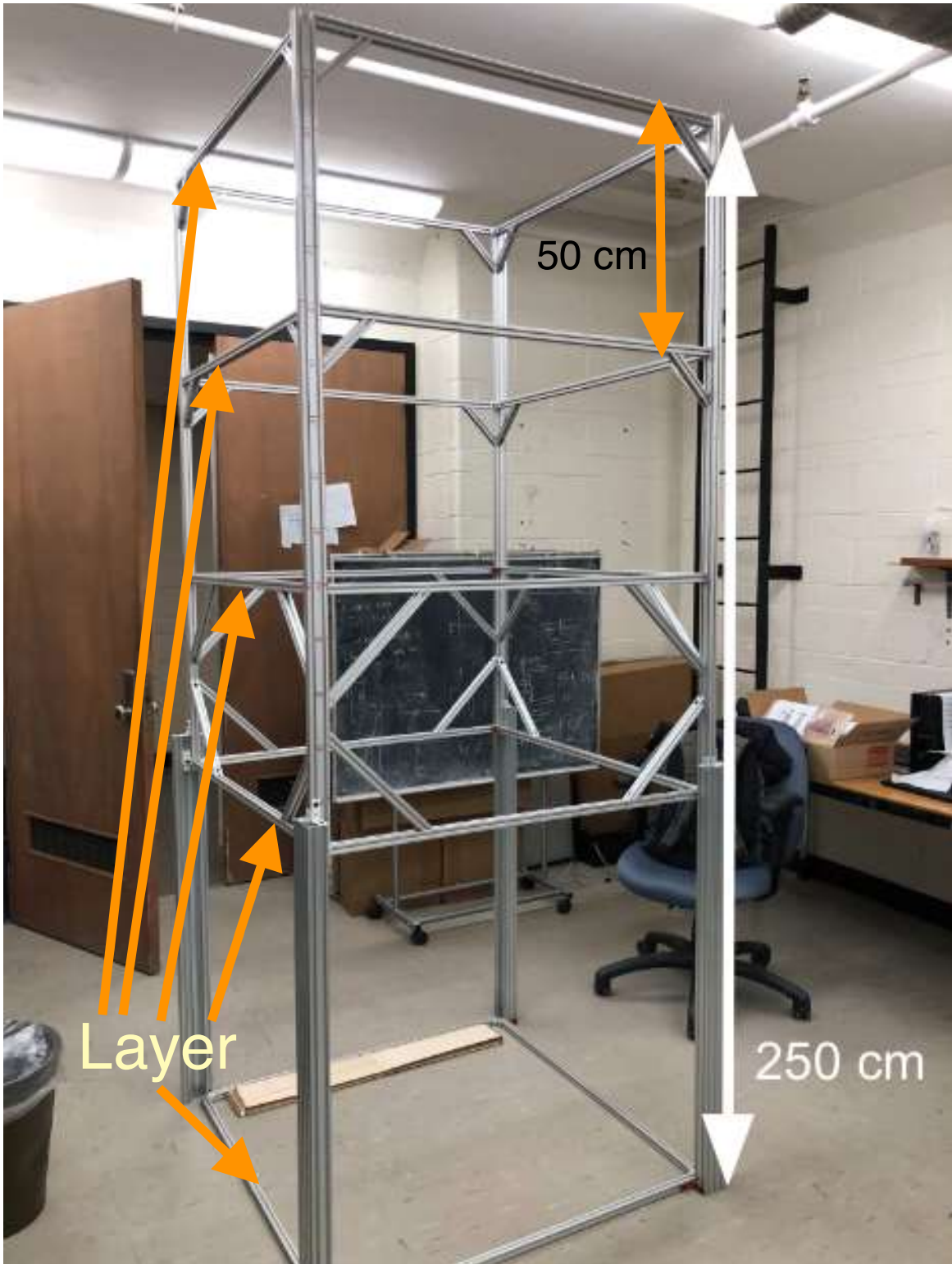
In the current design of the prototype module, less emphasis was placed on points 5 and 6. Point 5 is weighted less because there are currently not enough scintillator bars to sufficiently construct a layer and attach it to the prototype. Alternatives like substituting missing bars with dummy wood planks were rejected because the weight of the planks did not accurately represent the plastic scintillators. Without a layer, it is difficult to design the prototype for compatibility. In terms of the electronics, there are still some unknown problems with the DAQ that need to be debugged first. Moreover, readout boards — similar to the PCB that is shown in Figure 6 — to mount the SiPMs on have not yet been designed and fabricated. Accounting for cable management and testing different assemblies is difficult without the SiPM readout boards and a full scintillating layer for attaching electronics.

From points 1-4, the module that was designed is shown in Figure 19. The prototype module bears a close resemblance to the proposed MATHUSLA detector module — has 4 tracking layers and 1 bottom tracking layer. The distance between the lowest upper tracking layer and the bottom tracking layer serves as a "decay volume" like Figure 4 and is adjustable. The module has a profile of 95.5 cm × 95.5 cm and a height that varies from 150 cm to 250 cm. The module frame is built from single profile T-rails, double profile T-rails and C-rails. The single profile T-rails are attached to one of the profiles of the double profile T-rails — which act as the vertical stands. The connected T-rails form a square around the module frame and make up a layer. The second profile of the double profile T-rail enables the module

frame to slide and is connected to the C-rails; C-rails act as the legs of the module frame. In Figure 19, the double profile T-rails have a larger profile than the single profile ones (i.e. double profile have a rectangular appearance while single profile are squares).



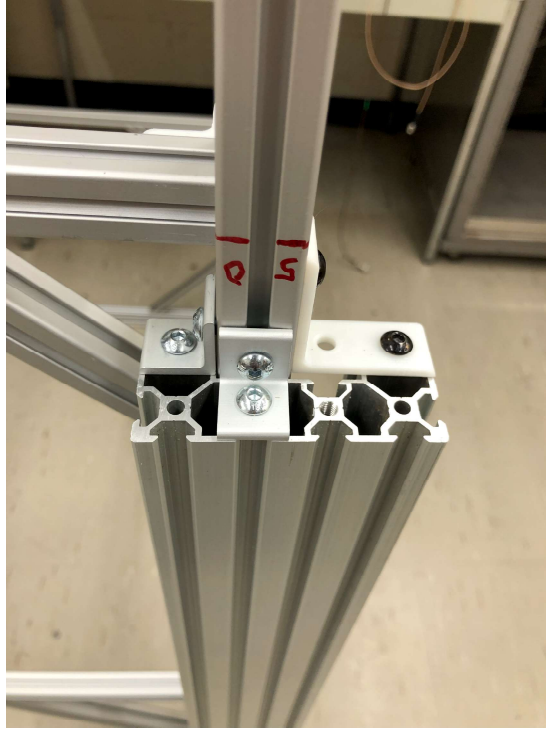
(a) Module frame at its lowest height



(b) Module frame at its max height. Labelled layers indicate rail sections where the scintillator layers would be attached to in the module

Figure 19: Prototype module frame at its lowest and tallest height

Height is controlled via corner connectors shown in Figure 20a and the height can be set according to the marking in Figure 20b. There are 4 sets of braking connectors seen in Figure 20a on the module frame — one placed at each leg of the frame.



(a) Braking mechanism for the module frame height. The center corner connector is the main load-bearing connector



(b) Height markings on the double T-rail to control the set height of the prototype module's upper layers

Figure 20: Height control of the prototype module

The entire module can support 5 scintillator layers. The upper 4 layers are spaced 50 cm apart as seen in Figure 19b and are attached to the double profile T-slot rail. The bottom layer is attached to the C-rail legs. The layer spacing between the bottom layer and the upper tracking layers can be adjusted via the height control mechanism. Additionally, spacing between the upper tracking layers can also be easily tuned by loosening the single profile T-rail connections to the frame and shifting them up or down to a desired new height.

The prototype does not collapse under its weight when the height is fully extended. An assortment of objects totalling an unknown weight was layered across the prototype at full size while the module was being pulled downwards. The frame was able to support that weight without collapsing.

A feature that can be included to help with the load bearing of the brakes is to fill

the gap between the double profile T-rail and C-rail in Figure 20b with the stopper piece shown in Figure 21. A stopper that is the entire length of the C-rail (or two stoppers half the length of the C-rail) can be slid in between the gap such that the white corner connector seen in Figure 20a rests on the top side of the stopper and the stopper's bottom face is on the ground. With the gap filled, the white connector can rest the load of the upper frame against the elongated stopper which is supported by the ground. This feature also has the added benefit of stabilizing any wobbling that might occur when the frame is fully extended. Wobbling and overall stability can be improved by including rubber feet on the bottom side of the C-rail legs.



Figure 21: Stopper piece to prevent the double profile T-slot rail from swinging out of the C-rail connection

The current prototype module design sufficiently addresses points 1-4. Additional testing may be required to determine how much weight the module frame can support at full height and if that is comparable to the weight of 4 scintillation layers. However, the prototype does serve as a good starting point for performing tests on the functionality and efficacy of the MATHUSLA detector module design.

3.2.2 Scintillator Layer Connection Piece

In the discussion of key consideration points for the prototype module under Sec 3.2.1, it was noted that there were not enough scintillator bars available to completely prototype a layer. Although a full layer could not be constructed, some initial design ideas for a connector piece to the frame were created. The main design consideration was that the scintillator bars should not need to be altered in order to attach them to the prototype module — hence, an external box-like design that the bars could be placed in would be optimal.

The proposed idea would be to line up the scintillator bars side-by-side along the length of a partially open box that serves as the base for the layer connection. The cover, another partially open box, is placed over the scintillator bars to help block out external light that might couple into the WLS fibres. The bars are assumed to be placed as tightly together as possible such that they will not shift around in the layer but do not cause the WLS fibres to bend at a radius smaller than its rated suggestion.

Figure 23 shows the proposed connector box design. The connector is composed of two parts: a cover and a base. Both cover and base are partially open box designs and are laser cut from 3 mm thick plywood. Each of the box designs cannot be cut from one single piece at its full length (i.e. cannot cut a piece that is 80 cm long) so they are divided into two parts (two 40 cm long parts) and later joined by snap-fit fingers as seen in Figure 22.

The box structure for the scintillator serves as an initial prototype. To make the attachment usable for layer construction, the sides — particularly the joints of the box — need to be reinforced with aluminum steel sheets to make the cover and base more rigid. One primary concern with using wood is that when the base may begin to flex once it starts to support the weight of the bars. The attachment bending will affect the levelling of the layer. Moreover, an improved design should include dividers on the base that would mark out where each scintillator bar be placed. Lastly, the attachment piece is not light-tight. The design shown in Figure 23 would need to be wrapped in some sort of insulation to prevent stray light from filtering in and coupling with the WLS fibres. Improvements can be made

to the proposed box structure once more scintillator bars are available to construct a layer.

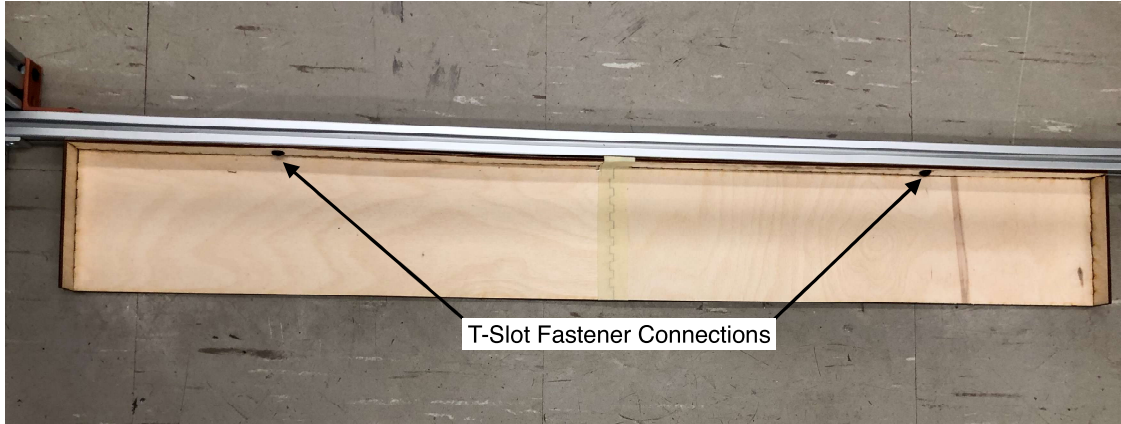


Figure 22: Base of the scintillator attachment piece. The snap-fit finger connection of two 40 cm long wood pieces is joined together as shown in the middle of the base. T-slot fasteners are used to attach the base of the scintillator attachment to the frame



Figure 23: Scintillator connector block to attach bars to the module frame. The connector block consists of a base and a top cover. Dimensions of the cover and base are shown in the figure. The height is 1.5 cm for both the cover and base

3.2.3 SiPM WLS Fibre Holder

The SiPM holder is necessary for creating an attachment piece that can couple the WLS fibre to the SiPM in a contained, light-tight box. There are 7 main design considerations for the SiPM holder:

1. **SiPM holder keeps the WLS fibre flush against the SiPM surface.** The SiPM's active detection region is the silicon diode surface shown in Figure 6. Since the fibre's circular profile is smaller than the diode surface, the fibre is able to direct more light created by the scintillator to a focused spot on the diode surface. However, if the fibre were to shift during operation, it would affect how much light is being directed to the SiPM. Thus, to ensure the same level of coupling during operation, the SiPM holder should have a mechanism that can keep the wire taut and flush against the SiPM.
2. **WLS fibre should not move around or be easy to pull.** Similar to point 1, the length of the WLS fibre threaded into the SiPM holder should not change to ensure the same coupling throughout the experiment. The SiPM holder should have a strong locking mechanism that prevents the WLS fibre from being pulled out or pushed further in when the lock is engaged.
3. **SiPM holder box should be easy to assemble.** Considering the number of SiPMs that the prototype module will have to support (at least 20 readout SiPMs per layer), a design that requires fewer parts to assemble will speed up installation onto the prototype module.
4. **SiPM holder box should be light-tight.** The SiPM holder will be coupling the WLS fibre to the SiPM. If the box is not light-tight, external sources may couple to the signal that is detected in the scintillator bar. Some possible outcomes may be that the SiPM does not trigger on the detected hit, triggers too early or cannot separate the true signal from external light. Hence, it is critical that the box design be either light-tight or easily light-proofed.
5. **SiPM holder profile should be similar to the scintillator bar profile for easy connection.** By keeping the two profiles similar, it will make threading the WLS fibre easier and reduce the chances of the fibre snapping. Moreover, keeping the same profile will also make it easier to light-proof the interface of the bar and holder.
6. **SiPM holder should be easy to connect and disconnect from the module**

frame like the scintillator layers. Similar to the layers of the prototype module (point 5 in Sec 3.2.1), there should be an easy interface to connect the SiPM holder to the module frame. However, the simple connection should not be chosen in favour of weakly attaching the holder to the module frame.

7. **SiPM holder has an easily accessible opening or mechanism to connect readout cables from SiPM to DAQ.** Since the SiPM is connected to a readout board, the holder should have some sort of opening that will allow cables to connect from the readout board to the DAQ. The opening should not be in a hard-to-reach place — for instance, in a gap between a single profile T-rail and the attached holder. Additionally, the opening to connect cables to the holder should not compromise the light-tightness of the interior.

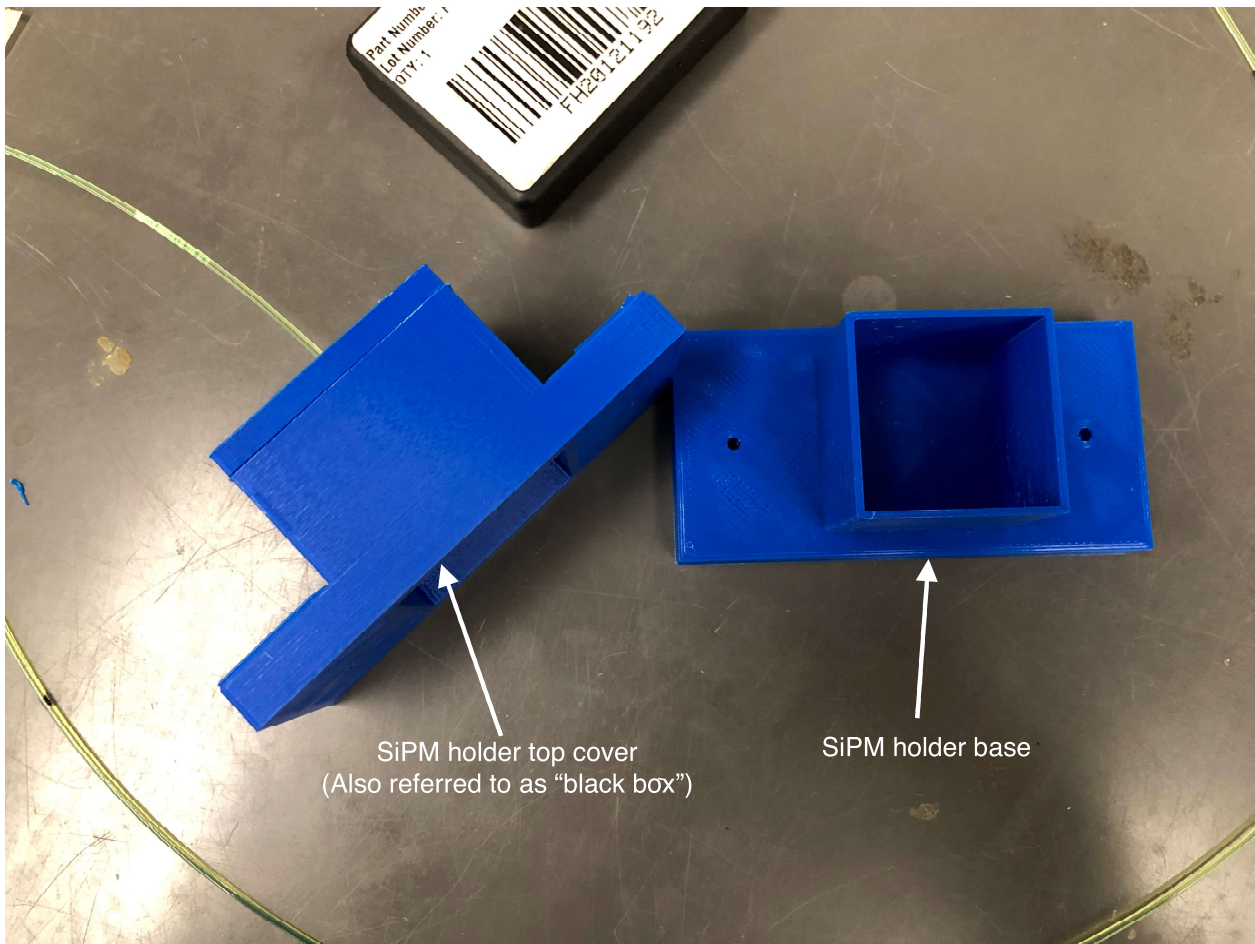


Figure 24: SiPM holder disassembled. The top cover (left) slots over the SiPM base (right). Screws are inserted into holes on the side flanges when the top cover is placed over the base and then tightened with nuts

Since we currently do not have the design for the SiPM readout board, point 7 is not heavily emphasized in the SiPM holder that was created. For the design, it was just assumed that the readout board of the SiPM would be 5 cm × 5 cm. No opening was designed for cable feed out because where pins would be located is unclear without the readout board.

The SiPM holder is shown in Figure 24. The profile of the SiPM holder (not including the flanges) is 5 cm × 5 cm and the height of the holder from the bottom of the holder base to the top of the holder cover is about 3.5 cm. The holder base is where the SiPM readout board would be attached — a possible location for the readout cabling would be to open up a hole at the bottom of the SiPM holder base. The WLS fibre is threaded through two plates and fed into the holder top cover or black box. In Figure 25, the WLS fibre on the inside of the SiPM cover is shown. The entire assembly is completed when the SiPM top cover is slotted over the base and nuts and screws are at the flanges to clamp the whole holder together.

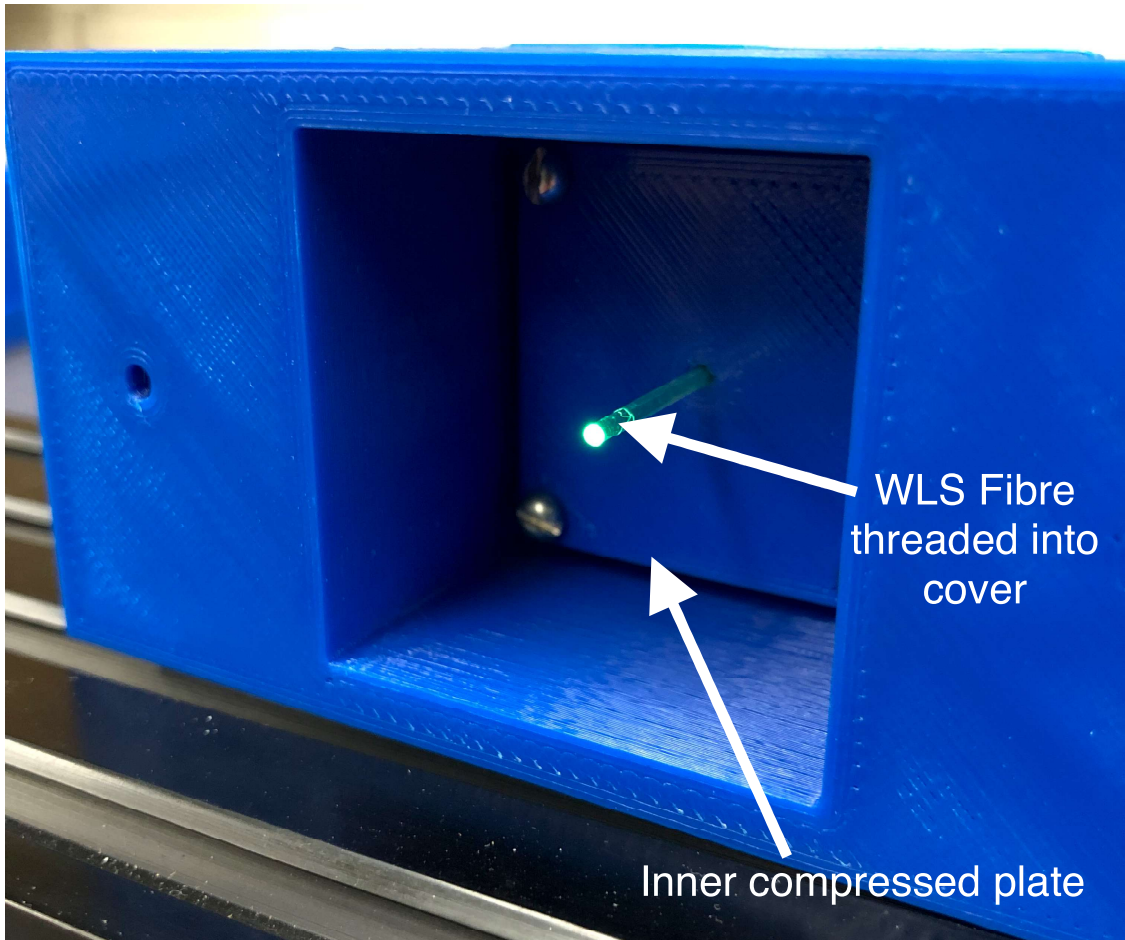


Figure 25: SiPM top cover interior with a WLS fibre threaded. The length of the fibre inside the top cover needs to be chosen before the plates are tightened

The WLS fibre is able to be held taut by the SiPM holder's top cover by compressing O-rings. O-rings with an inner diameter of 0.042" and an outer diameter of 0.140" were used for WLS fibre with a diameter of 1.5 mm. An exploded view of the assembly is shown in Figure 26.

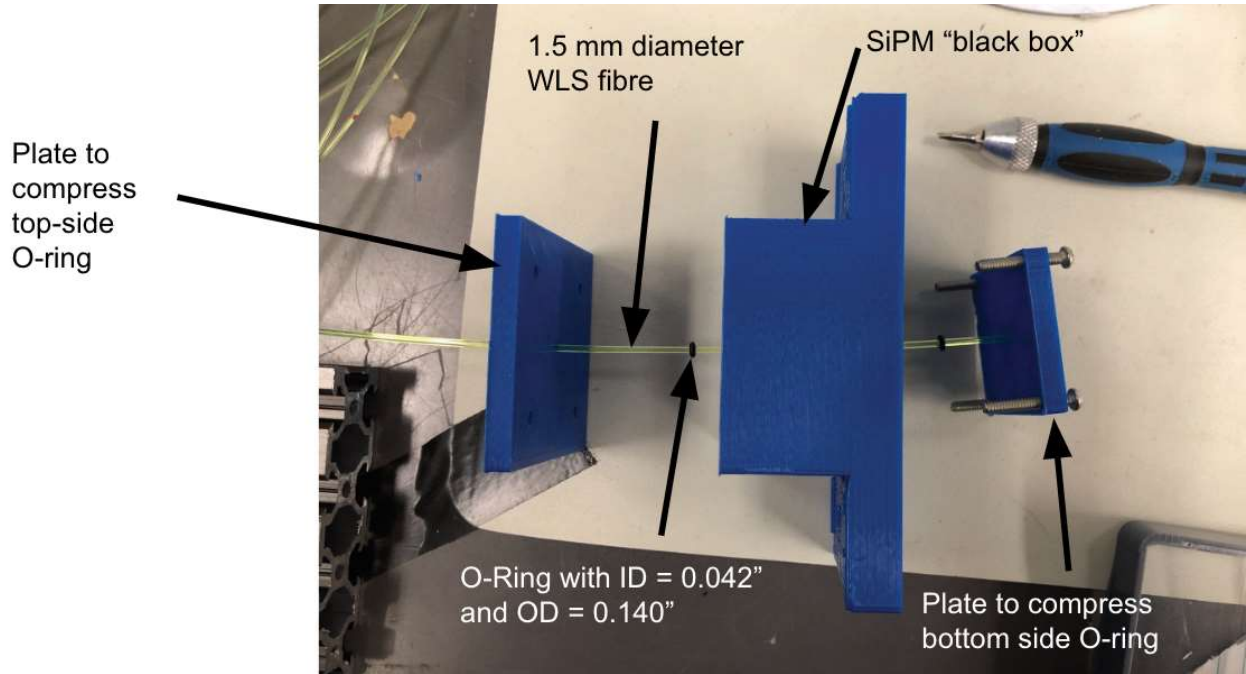


Figure 26: Exploded view of how the WLS wire is threaded into the SiPM top cover. Once the desired length of the WLS fibre is reached in the interior of the holder's black box, the two inner and outer plates are firmly together to sandwich the O-rings

The compression of the O-rings between the plate and the holder's top cover causes it to tighten around the WLS fibres and hold it in place. Therefore, the fibre will not shift around and can maintain its coupling to the SiPM readout board when the holder is base connected. In the design of the SiPM holder, the WLS fibre is chosen with a 1.5 mm diameter. A different-sized fibre would require new O-rings and a change in the hole diameter on the holder. It is possible to make the design more adaptable by using four compressive plates rather than two. Then, the fibre would be compressed between the plates rather than a plate and the holder. Different plate hole diameters would be able to support WLS fibres of many diameters.

Lastly, Figure 27 shows a sample assembly of 2 scintillating bars with the SiPM holder. Note that the scintillating bars used have the right profile dimensions, but there are two holes drilled for threading two fibres instead of only one hole for one fibre. In the mock assembly, it can be seen that having the holder maintain the same profile as the scintillator bar will

make it easier to light-proof the point where the two meet. Moreover, it is easier to align the scintillator bar to the SiPM connector piece when the two have the same profile shape. In Figure 27, the holder is quite not centred on the bar's face due to the bar being designed for a two-fibre input as opposed to a single input.

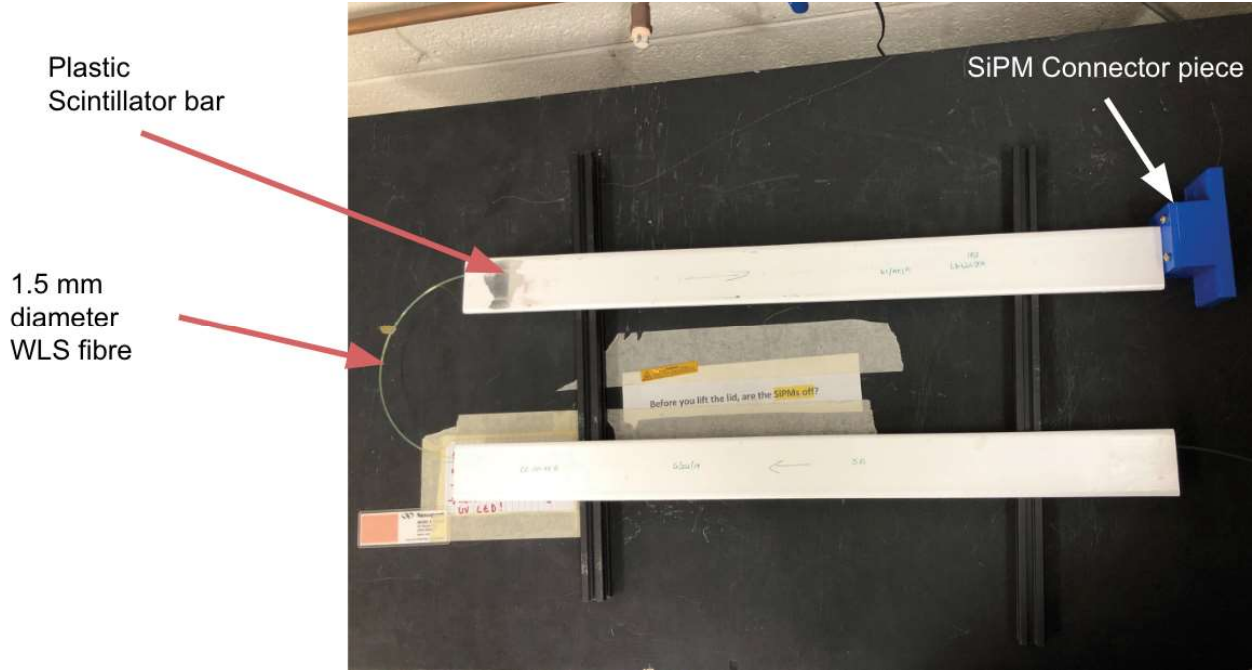


Figure 27: Sample mock-up of the assembly of two scintillator bars with a SiPM holder connected to one bar. In the prototype module, there would be one SiPM holder for every scintillator bar

Overall, the proposed SiPM holder design can satisfy points 1-6 of the design considerations. Note that point 6 can be easily met by replacing the nuts that would tighten the flanges of the holder with T-slot fasteners. The proposed approach would make it easy to connect and remove the holder. Point 7 of the design criteria was not weighed heavily when creating the current prototype. Once a sample readout board design has been made, it should be relatively simple to make adjustments to either the holder's base or the holder's top cover to accommodate for readout cabling. Furthermore, it would also be relevant to assess how well the SiPM holder design will integrate with the implementation of the scintillator layer. Some changes may be required so that the scintillator layers can be level with the floor and aligned with the holder.

4 Conclusion

4.1 Summary of Results and Developments

In this thesis work, the most significant results and outcomes are summarized as follows:

1. **Evaluation of the commercial CAEN DAQ board's ASIC channel failure rate.** See Sec 3.1.1. It was found that a total of 12 channels out of 64 readout channels were broken — about 20% of channels were unusable. The failure rate of channels seemed to be about 1 per month. A newly shipped DAQ saw 4 channels shorted together and 2 ASIC chips (a total of 64 channels) becoming inoperable during data collection. This occurred within 2 weeks of receiving the new DAQ. The causes for channel failure are unknown at the time of this thesis work.
2. **Noise Reduction of SiPM readout.** See Sec 3.1.2. The dominant cause of pre-amplifier signal noise was identified to be the quality of the cabling that connected a SiPM to the DAQ board. Comparisons of the pre-amplifier pulse signal output by the DAQ board showed larger amplitudes of low-frequency (10-100 MHz) noise coupled into the pre-amplifier signal. Exchanging a low-quality coaxial cable for a high-quality one saw a substantial reduction in low-level noise.
3. **Time of flight measurements with CAEN DAQ board.** See Sec 3.1.3. The ToF measurements measured the time difference for two SiPMs to be triggered by laser pulses. Each SiPM had one laser pulse source to stimulate it — the laser pulsars were generated by separate sources, but they were being driven with the same pulsing frequency. It was found that the ToF measurements were able to reach ~ 1 ns resolution. However, distributions of the ToF were not Gaussian and further investigation identified an irregular fine time distribution as being the main cause. Currently, there is no solution to this problem as of this thesis work.
4. **Prototype Module Construction.** See Sec 3.2.1. A small prototype module that replicates the design of the proposed MAHTHULSA detector module [4, 21, 23] was constructed. The prototype module delivers a design that can support a total of five scintillating tracking layers and has modular components for easy adjustment of the frame to suit different testing requirements. The design did not place emphasis on the integration of scintillating layers into the frame nor did it consider cable management and where to mount the DAQ board.

5. **Proposed scintillator layer attachment design.** See Sec 3.2.2. A layer attachment blueprint was drafted and then laser cut. The proposed layer attachment would be to use one open-faced box as a base to place scintillator bars on and the second open-faced box would act as a cover to prevent external light sources from coupling into the WLS fibres. The layer attachment is mounted to the prototype module frame with T-slot fasteners. At the time of the thesis, this is a rudimentary prototype.
6. **Silicon photomultiplier holder for improved WLS fibre coupling.** See Sec 3.2.3. A 3D-printed SiPM holder design was created. The component was able to effectively keep a WLS fibre threaded through it taut and held stationary. Moreover, the component assembly was simple and straightforward and could maintain a light-tight interior with some minimal light-proofing. The SiPM holder design was untested in how well it would integrate with a complete scintillator layer.

The first half of the thesis was aimed at the evaluation of a commercial DAQ system. A system like the CAEN DAQ is able to support up to 128 SiPM readout channels — this makes it easily scalable when many readouts are needed. This makes it a convenient solution for integrating the readout of many SiPMs (as required in MATHUSLA). However, if the DAQ system is unable to provide the necessary measurement resolution or suffers from constant breakage then an alternative should be considered. The work that was completed in this thesis to study the failure rate of ASIC channels and the resolution of ToF measurements will give valuable information about whether the CAEN system is a good option for use in MATHUSLA.

The project's second half was devoted to the development of a testable prototype module. The proposed MATHUSLA detector modules will each be $9\text{ m} \times 9\text{ m} \times 30\text{ m}$ in size. It will be particularly hard to make changes or study certain aspects at the scale of the actual module. Hence, a small-scale local module offers a flexible solution for optimizing and testing different configurations. This thesis lays the groundwork for an apparatus that can be utilized in future tests to investigate the behaviour of the MATHUSLA detector module on a limited scale.

4.2 Future Work

A lot of the work completed in the thesis is relatively new — the mechanical designs in particular. Improvements to the mechanical design will assist in setting up small-scale tests using the prototype module. Additionally, there are still some more tests that can be

done to assess the quality and performance of the CAEN DAQ system. Some of the possible next-step items are mentioned:

- **Testing of the CAEN DAQ with improved SiPMs.** The SiPMs that were used in this thesis project are generic off-the-shelf quality devices. As a result, their performance may not be optimized. In consultations with engineers at CAEN, they have suggested that a slow SiPM output (i.e. requires more than 5 ns to reach its peak value in the pre-amplifier signal) can cause the abnormal fine time distribution that was observed. An extension then would be verifying the performance of the DAQ with higher quality SiPMs from a company like Hamamatsu.
- **Module and SiPM holder wiring designs.** As mentioned, the current iterations of these designs do not take into account the cable management or connections to the DAQ from the SiPMs in the scintillator layers. The next step in the mechanical design of the SiPM holder would be to identify where cable feed-throughs could be added — it is important to remember that the feed-through openings should either preserve the light-tightness of the holder’s interior or also be easily light-proofed. With regard to the prototype module’s frame, the DAQ mounting needs to be figured out. Another layer for the DAQ cannot be inserted between the tracking layers which means that the DAQ must be mounted on either the frame or by some other component. Additionally, the DAQ system should be mounted in such a way that the length of cables connected to the DAQ is as short as possible to avoid noise coupling into the SiPM readout signals.
- **Scintillator layer attachment.** The current scintillator attachment piece is a very rough design. Without enough bars to build a complete scintillating layer, it is a bit difficult to design an optimal connecting piece. However, as a next step, the current attachment piece can be improved upon by considering how to light-proof the enclosure, combining the cover and base and deciding how cables should be connected to the layer.
- **Module and SiPM holder light-proofing.** The importance of the SiPM holder being shielded against external sources of light is critical to the performance of the overall detector. A small extension on the SiPM holder design would be to spot any locations where light may leak in and seal it — either with a new design or with some external material. Similarly, the prototype detector module should also be light-proofed to an extent. Assessing solutions for light-proofing the attachments or gaps in the scintillating layers that expose the WLS fibre is another important next step.

Bibliography

- [1] J. Alimena *et al.*, “Searching for long-lived particles beyond the Standard Model at the Large Hadron Collider,” *J. Phys. G*, vol. 47, no. 9, p. 090501, 2020.
- [2] D. Curtin *et al.*, “Long-Lived Particles at the Energy Frontier: The MATHUSLA Physics Case,” *Rept. Prog. Phys.*, vol. 82, no. 11, p. 116201, 2019.
- [3] “The Large Hadron Collider.” [Online]. Available: <https://www.home.cern/science/accelerators/large-hadron-collider>
- [4] “The MATHUSLA experiment.” [Online]. Available: <https://mathusla-experiment.web.cern.ch/>
- [5] “DT5550W - complete readout system based on Weeroc ASIC - Caen - Tools for Discovery,” Mar 2022. [Online]. Available: <https://www.caen.it/products/dt5550w/>
- [6] G. Aad *et al.*, “The ATLAS Inner Detector commissioning and calibration,” *Eur. Phys. J. C*, vol. 70, pp. 787–821, 2010.
- [7] E. Le Boulicaut, “The Standard Model.” [Online]. Available: <https://cds.cern.ch/record/2759492/files/Standard%20Model%20-%20ATLAS%20Physics%20Cheat%20Sheet.pdf>
- [8] S. Shirai, “Theory Overview: Why are Long-lived particles important?” [Online]. Available: <https://indico.cern.ch/event/851166/contributions/3599446/attachments/1949527/3235593/overview.pdf>
- [9] L. Lee, C. Ohm, A. Soffer, and T.-T. Yu, “Collider searches for long-lived particles beyond the Standard Model,” *Progress in Particle and Nuclear Physics*, vol. 106, pp. 210–255, 2019. [Online]. Available: <https://doi.org/10.1016%2Fj.pnpp.2019.02.006>
- [10] M.-H. Genest, “Searching for long-lived BSM particles at the LHC.” [Online]. Available: http://www.scholarpedia.org/article/Searchng_for_Long-Lived_BSM_Particles_at_the_LHC
- [11] J. L. Feng, “Naturalness and the status of supersymmetry,” *Annual Review of*

- Nuclear and Particle Science*, vol. 63, no. 1, pp. 351–382, 2013. [Online]. Available: <https://doi.org/10.1146/annurev-nucl-102010-130447>
- [12] “Planck length: Cosmos.” [Online]. Available: <https://astronomy.swin.edu.au/cosmos/p/Planck+Length>
- [13] N. Craig, “Naturalness hits a snag with higgs,” Nov 2020. [Online]. Available: <https://physics.aps.org/articles/v13/174>
- [14] M. Gomez-Bock, M. Mondragon, M. Mühlleitner, R. Noriega-Papaqui, I. Pedraza, M. Spira, and P. M. Zerwas, “Electroweak symmetry breaking and higgs physics: basic concepts,” *Journal of Physics: Conference Series*, vol. 18, no. 1, p. 74, jan 2005. [Online]. Available: <https://dx.doi.org/10.1088/1742-6596/18/1/002>
- [15] C. Csaki, “The Minimal supersymmetric standard model (MSSM),” *Mod. Phys. Lett. A*, vol. 11, p. 599, 1996.
- [16] M. F. Sohnius, “Introducing supersymmetry,” *Physics Reports*, vol. 128, no. 2, pp. 39–204, 1985. [Online]. Available: <https://www.sciencedirect.com/science/article/pii/0370157385900237>
- [17] A. H. G. Peter, “Dark Matter: A Brief Review,” *arXiv e-prints*, p. arXiv:1201.3942, Jan. 2012.
- [18] K. Garrett and G. Duda, “Dark Matter: A Primer,” *Adv. Astron.*, vol. 2011, p. 968283, 2011.
- [19] N. Bernal, M. Heikinheimo, T. Tenkanen, K. Tuominen, and V. Vaskonen, “The Dawn of FIMP Dark Matter: A Review of Models and Constraints,” *Int. J. Mod. Phys. A*, vol. 32, no. 27, p. 1730023, 2017.
- [20] V. Khachatryan *et al.*, “Search for Heavy Stable Charged Particles in pp collisions at $\sqrt{s} = 7$ TeV,” *JHEP*, vol. 03, p. 024, 2011.
- [21] C. Alpigiani *et al.*, “An Update to the Letter of Intent for MATHUSLA: Search for Long-Lived Particles at the HL-LHC,” 2020. [Online]. Available: <https://doi.org/10.48550/arXiv.2009.01693>

- [22] J. Barron and D. Curtin, “On the Origin of Long-Lived Particles,” *JHEP*, vol. 12, p. 061, 2020.
- [23] C. Alpigiani *et al.*, “Recent Progress and Next Steps for the MATHUSLA LLP Detector,” in *2022 Snowmass Summer Study*, Mar 2022.
- [24] M. Suffert, “Silicon photodiode readout of scintillators and associated electronics,” *Nuclear Instruments and Methods in Physics Research Section A: Accelerators, Spectrometers, Detectors and Associated Equipment*, vol. 322, no. 3, pp. 523–528, 1992. [Online]. Available: <https://www.sciencedirect.com/science/article/pii/016890029291226Y>
- [25] *Basic Principles of Photomultiplier Tubes*, 3rd ed. Hamamatsu Photonics, 2007, p. 13–19. [Online]. Available: https://www.hamamatsu.com/content/dam/hamamatsu-photonics/sites/documents/99_SALES_LIBRARY/etd/PMT_handbook_v3aE.pdf
- [26] A. Peisert, “Silicon Microstrip Detector,” 1992. [Online]. Available: <http://cds.cern.ch/record/2627234>
- [27] “ON Semiconductor, Introduction to the Silicon Photomultiplier (SiPM), AND9770/D,” Jul 2021. [Online]. Available: <https://www.onsemi.com/pub/Collateral/AND9770-D.PDF>
- [28] “Plastic scintillators.” [Online]. Available: <https://www.crystals.saint-gobain.com/radiation-detection-scintillators/plastic-scintillators#:~:text=The%20scintillation%20emission%20of%20a,time%20of%20around%202%20ns>.
- [29] “Fibers.” [Online]. Available: <https://www.crystals.saint-gobain.com/radiation-detection-scintillators/fibers>

